Autotrophic denitrification supported by sphalerite and oyster shells: Chemical and microbiome analysis

Erica Dasi, Jeffrey Cunningham, Emmanuel Talla, Sarina Ergas

▶ **To cite this version:**

Erica Dasi, Jeffrey Cunningham, Emmanuel Talla, Sarina Ergas. Autotrophic denitrification supported by sphalerite and oyster shells: Chemical and microbiome analysis. Bioresource Technology, 2023, 375, pp.128820. 10.1016/j.biortech.2023.128820 . hal-04028017

HAL Id: hal-04028017
https://amu.hal.science/hal-04028017

Submitted on 9 Oct 2023

HAL is a multi-disciplinary open access archive for the deposit and dissemination of scientific research documents, whether they are published or not. The documents may come from teaching and research institutions in France or abroad, or from public or private research centers.

L'archive ouverte pluridisciplinaire **HAL**, est destinée au dépôt et à la diffusion de documents scientifiques de niveau recherche, publiés ou non, émanant des établissements d'enseignement et de recherche français ou étrangers, des laboratoires publics ou privés.

Autotrophic denitrification supported by sphalerite and oyster shells: Chemical and microbiome analysis

Erica A. Dasi[a], Jeffrey A. Cunningham[a], Emmanuel Talla[b], Sarina J. Ergas[a*]

a. Department of Civil & Environmental Engineering, University of South Florida (USF), 4202 E. Fowler Ave, ENG 030, Tampa, FL 33620, USA

b. Aix Marseille Univ, CNRS, Laboratoire de Chimie Bactérienne (LCB), F-13009, Marseille, France

*__Corresponding author__:

sergas@usf.edu (S.J. Ergas); Address: 4202 E. Fowler Avenue, ENG 030, Tampa, FL 33620-5350, USA

Abstract

This research evaluated the metal-sulfide mineral, sphalerite, as an electron donor for autotrophic denitrification, with and without oyster shells (OS). Batch reactors containing sphalerite simultaneously removed NO_3^- and PO_4^{3-} from groundwater. OS addition minimized NO_2^- accumulation and removed 100% PO_4^{3-} in approximately half the time compared with sphalerite alone. Further investigation using domestic wastewater revealed that sphalerite and OS removed NO_3^- at a rate of 0.76 ± 0.36 mg NO_3^--N/(L · d), while maintaining consistent PO_4^{3-} removal (~97%) over 140 days. Increasing the sphalerite and OS dose did not improve the denitrification rate. 16S rRNA amplicon sequencing indicated that sulfur-oxidizing species of *Chromatiales*, *Burkholderiale*s, and *Thiobacillus* played a role in N removal during sphalerite autotrophic denitrification. This study provides a comprehensive understanding of N removal during sphalerite autotrophic denitrification, which was previously unknown. Knowledge from this work could be used to develop novel technologies for addressing nutrient pollution.

Keywords: Sphalerite, Oyster shells, Autotrophic denitrification**,** Phosphorus removal**,** 5-Stage Bardenpho microbiome

1. Introduction

Pollution of ground and surface waters by the nutrients nitrogen (N) and phosphorus (P) remains a major cause of eutrophication and can increase the risk of methemoglobinemia, specific cancers, and birth defects in humans (Ward et al., 2018). Nutrient sources include poorly functioning centralized or onsite wastewater treatment facilities, fertilizers, livestock wastes, and urban and agricultural runoff. Small community water systems (CWS) have limited access to technological and financial resources for nutrient control, making them especially vulnerable to N and P pollution (Gasteyer, 2010). For example, more than 5,000 small CWS in the US violated the federal maximum contaminant level of 10 mg/L NO_3^--N in 2013 (Oxenford and Barret, 2016). Nutrient control is therefore essential to preserve water resources, especially in small community settings.

Autotrophic denitrification is a promising approach to treat NO_3^--contaminated waters (Hu et al., 2020). Autotrophic denitrifiers use inorganic electron donors, such as hydrogen gas (Ergas and Reuss, 2001) or elemental sulfur (S^0) (Sengupta et al., 2007), and inorganic carbon sources for cell synthesis. In some contexts, the use of inorganic electron donors reduces secondary contamination that can occur when organic carbon is carried over to the product water (Ergas and Aponte-Morales, 2014). Autotrophic denitrifiers also have low sludge production rates due to their slow growth yields (Sierra-Alvarez et al., 2007). This may lower backwashing and sludge disposal costs for certain denitrification designs (e.g., packed or fluidized beds; Hu et al., 2020). Thus, overall, autotrophic denitrification may offer an inexpensive and low-complexity approach to address nutrient pollution in various settings.

Metal sulfide minerals, such as pyrite (FeS_2) and pyrrhotite ($Fe_{(1-x)}S$ (x = 0 to 0.2)), are widespread and abundant in the earth's crust and have attracted interest for autotrophic denitrification (Li et al., 2013; Kong et al., 2016; Li et al., 2016; Ge et al., 2019; Hu et al., 2020).

These minerals can be used as both slow-release electron donors and biofilm carriers in packed-bed reactors (Tong et al., 2017). Pu et al. (2014) observed NO_3^- removal efficiencies exceeding 99% in batch pyrite denitrification reactors used for treating groundwater. Metal sulfide minerals can also support simultaneous NO_3^- and P removal by forming hydroxides (e.g., $Fe(OH)_3$) that promote PO_4^{3-} adsorption (Li et al., 2013; 2016). Li et al. (2013) observed NO_3^- and PO_4^{3-} removal efficiencies exceeding 99% in ferrous sulfide (FeS) batch reactors applied to treat wastewater. Furthermore, a pyrrhotite autotrophic denitrification biofilter was shown to remove 96% of both total oxidized nitrogen and PO_4^{3-} from wastewater (Li et al., 2016). The success of pyrite, ferrous sulfide, and pyrrhotite in supporting nutrient removal suggests that other previously untested metal sulfide minerals might have this capability. Sphalerite ((Zn,Fe)S) might be a promising substrate for denitrification as it primarily contains sulfide (32-33%). Its trace mental content may also support PO_4^{3-} removal (45-67% zinc, ≤ 18% iron, ≤ 28% cadmium, and ≤ 3% manganese; Anthony et al., 1990).

Oyster shells are a widespread by-product of the global shellfish industry and can be applied as a low-cost material to support N and P removal from water. They are composed of approximately 97% calcium carbonate in a scleroprotein matrix (Asaoka et al., 2009). Oyster shells enhance sulfur-driven autotrophic denitrification by serving as a slow-release alkalinity source (Sengupta et al., 2007), surface for biofilm attachment (Tong et al., 2017), and possibly an organic carbon source for mixotrophic (i.e., mixed autotrophic and heterotrophic) denitrification (Asaoka et al., 2009; Tong et al., 2017). Previous research demonstrated that a pyrite-based autotrophic denitrification biofilter containing oyster shells achieved a higher NO_3^- removal efficiency (90%) and lower SO_4^{2-} production (150 mg/L) than pyrite alone (Tong et al., 2017). Oyster shells were also shown to achieve long-term (210 d) PO_4^{3-} removal (96%) when applied as an adsorbent (Park and Polprasert, 2008).

Prior studies have investigated the microbial community structure in denitrifying systems with metal sulfide minerals to understand the biological mechanisms of N removal (Pu et al., 2014; Kong et al., 2016; Li et al., 2016). *Thiobacillus* is the most reported sulfur-oxidizing and denitrifying genus in laboratory and pilot-scale studies with pyrite and pyrrhotite (Kong et al., 2016; Li et al., 2016; Ge et al., 2019). Kong et al. (2016) are, to date, the only authors that have explored the microbial community structure when sulfur (S) mineral and oyster shells are combined. The authors confirmed that mixotrophic processes occurred in a pyrite and oyster shell-based biofilter by the presence of both autotrophic and heterotrophic bacteria, such as *Thiobacillus* and *Thauera*, respectively (Kong et al., 2016).

Multiple research gaps exist regarding the use of metal sulfide minerals for autotrophic denitrification. First, no prior published studies have investigated the use of sphalerite as an electron donor for autotrophic denitrification. Second, few studies have investigated the combined effect of oyster shells and metal sulfide minerals on autotrophic denitrification. Based on a review of the prior literature, pyrite is the only metal sulfide mineral that has been studied in conjunction with oyster shells (Tong et al. 2017; 2018; Kong et al., 2016). Third, no reports have explored the contribution of the microbial community to denitrification when oyster shells and metal sulfide minerals other than pyrite are combined. Expanding knowledge in these areas can help researchers identify appropriate substrates to use in autotrophic denitrifying technologies.

The broad goal of this research is to improve the understanding of metal sulfide mineral-based denitrification to support the development of novel technologies that can address nutrient pollution globally. The specific objectives are to: (1) Examine the denitrification performance of sphalerite by quantifying NO_3^- and PO_4^{3-} removal as well as by monitoring SO_4^{2-} by-product formation; (2) Evaluate the effect of combining sphalerite and oyster shells on denitrification performance; (3) Assess the effect of sphalerite and oyster shell dose on denitrification

performance; and (4) Uncover the microbial community during sphalerite autotrophic denitrification, with and without oyster shells, to understand N-transformations as well as N removal mechanisms.

2. Materials and methods

Work was completed in three phases, each employing batch reactor studies. Phase 1 investigated the denitrification performance of sphalerite using groundwater contaminated by NO_3^- and PO_4^{3-}. Phase 2 evaluated the effect of oyster shell addition on the removal of both NO_3^- and PO_4^{3-} from groundwater. Phase 3 assessed the effect of sphalerite and oyster shell dose on nutrient removal in a larger scale reactor with nitrified domestic wastewater instead of groundwater. The microbial community was characterized in each phase to elucidate the N-transformations and N removal mechanisms linked to sphalerite autotrophic denitrification.

2.1 Materials

Sphalerite was obtained from Fisher Scientific (Waltham, Massachusetts) for use in Phases 1 and 2. Sphalerite from the Middle Tennessee Mines was used for Phase 3 (Nyrstar Corporation, Budel, Netherlands). Oyster shells were purchased from a local agricultural supplier (Shells, Tampa, Florida). S^0 pellets (4.0–6.0 mm; 90% sulfur and 10% bentonite), which were used as a positive control, were obtained from Southern Aggregates (Palmetto, Florida). Sphalerite samples were characterized using powder X-ray diffraction as described by Dasi (2022). X-ray patterns confirmed the presence of sphalerite in both sources (Dasi, 2022). Sphalerite and oyster shells were crushed manually and sieved to a particle size between 1-2 mm. The crushed minerals were pre-treated as described by Pu et al. (2014) prior to use in reactors. Briefly, the crushed minerals were soaked in a 10% (v/v) hydrochloric acid solution, rinsed with

deionized water, dried at 103 °C, and maintained under anoxic conditions until use. Oyster shells were rinsed with deionized water and dried at 20 ± 2 °C.

2.2 Inoculum and water sources

Settled mixed liquor suspended solids (MLSS) were collected from the Hillsborough County Northwest Regional Water Reclamation Facility (NWRWRF; Tampa, Florida), which applies a five-stage Bardenpho process for biological nutrient removal. For all phases, the MLSS was used as an inoculum source containing a diverse microbial community to select a unique consortium of denitrifying bacteria that oxidize sphalerite (Zhou et al., 2017). Groundwater from the University of South Florida's Botanical Gardens (0.8 ± 0.69 mg/L NO_3^--N, 0.0 ± 0.0 mg/L NH_4^+-N, 1.1 ± 1.1 mg/L PO_4^{3-}-P, 173.6 ± 33.6 mg/L alkalinity [as $CaCO_3$], and 12.5 ± 2.5 mg/L chemical oxygen demand [COD]) was used as a water source for Phases 1 and 2.The groundwater was filtered through a 0.45-µM mixed cellulose ester membrane (Fisher Scientific, Waltham, Massachusetts) before use. Secondary clarifier effluent collected from the Hillsborough County Northwest Regional Water Reclamation Facility was used as a domestic wastewater source in Phase 3. Analytical-grade KNO_3, $NaHCO_3$, NH_4Cl, K_2HPO_4, and KH_2PO_4 (Fisher Scientific, Waltham, Massachusetts) were added to the water sources to achieve initial target concentrations of approximately 40–100 mg/L NO_3^--N, 300 mg/L alkalinity as $CaCO_3$, 1–10 mg/L NH_4^+-N, and 1–10 mg/L PO_4^{3-}-P, respectively.

2.3 Batch reactor setup

Table 1 provides information on the batch studies. Phase 1 and 2 batch reactors were constructed using 250 mL glass anaerobic serum bottles with septum seal crimp caps. To investigate the effect of system scale and sphalerite mass on denitrification performance, Phase 3 batch reactors were constructed in 1 L glass bottles with screw caps drilled to fit two 5-mL plastic

pipettes. The first pipette served as a sampling port to withdraw liquid. The second pipette allowed the headspace to be connected to a FlexFoil gas sample bag (SKC, Inc., Eighty-Four, Pennsylvania) containing N_2 gas. This allowed the reactors to remain anoxic as liquid samples were removed from the bottles. In all three phases, reactors (except for uninoculated controls) were inoculated with 300 mg/L volatile suspended solids from the NWRWRF. All inoculated reactor types in the first two phases were tested in triplicate. Single batch reactors were assembled to test each uninoculated (UN) control during Phases 1 and 2 as well as the experimental and control samples of Phase 3. Following construction and inoculation, reactors were flushed with N_2 gas for 7 min to provide anoxic conditions, then incubated in a dark constant-temperature room at 22 ± 2 °C.

In Phase 1, denitrification was monitored in four types of batch reactors: (a) Experimental reactors containing sphalerite were used to assess its ability to support nutrient removal by autotrophic denitrification; (b) Positive controls containing S^0 and oyster shells (OS) were used as a basis of comparison to assess the performance of sphalerite; (c) An uninoculated (UN) reactor, containing sphalerite but without MLSS, was used as a negative control to test for abiotic removal of NO_3^- and PO_4^{3-}; and (d) Inoculum-only control reactors, which were inoculated with MLSS but did not contain sphalerite or OS, were used to test for heterotrophic denitrification supported by endogenous decay of the MLSS.

In Phase 2, denitrification was examined using an inoculum-only control and three different types of batch reactors: (a) Experimental reactors containing sphalerite and OS were combined at a 3:1 mass ratio (Table 1) to evaluate the effect of combining these substrates on nutrient removal; (b) Reactors containing OS and MLSS were used to assess if biological nutrient removal can be supported by OS alone; and (c) an UN reactor containing OS was used to test for abiotic reactions induced by the OS.

In Phase 3, denitrification was investigated over three cycles. In cycle 1, sphalerite and OS were added a 4:1 ratio (Table 1). After 30 days, additional sphalerite and OS were added to evaluate the effect on denitrification performance for two additional cycles. This phase also employed the inoculum-only control as described above. Whenever the NO_3^- concentration in the reactors fell below 6 mg/L (as N) during Phase 3, half of the liquid volume was replaced with the fresh prepared wastewater to begin another cycle.

2.4 Sampling and Analysis

Samples of supernatant were collected and filtered through 0.45-µM membrane filters (Fisher Scientific, Waltham, MA) for measurement of anions, cations, total N (TN), total P (TP), and COD. Anions and cations were measured using 881 Compact IC Pro anion or cation ion chromatography systems (Metrohm AG, Herisau, Switzerland) based on *Standard Methods* 4110B (APHA et al., 2017). TN, TP, and COD were measured using the HACH methods 827, 844, and 8000, respectively. Unfiltered liquid samples were used to measure alkalinity and pH using *Standard Methods* 2320B (APHA et al., 2017) and a calibrated Orion 5-Star meter (Thermo Scientific, Beverly, MA). Samples were collected for DNA extraction to examine the microbial community on the days listed in Table 1. MLSS samples were also collected from the NWRWRF to characterize the initial microbial community of the wastewater inoculum and to evaluate the microbial community change over time.

2.5 Microbial community analysis

16S rRNA amplicon sample preparation and sequencing were performed as described by He et al. (2021). Briefly, genomic DNA was extracted according to the manufacturer's instructions of the AllPrep PowerViral DNA/RNA Kit (QIAGEN, INC., Hilden, Germany). PCR amplification, library preparation, and sequencing were performed by Applied Biological

Materials, Inc. (Vancouver, Canada). The raw sequencing reads were deposited into the NCBI Sequence Read Archive database under the accession numbers: PRJNA830589 and PRJNA926698.

Processing of the raw sequencing data was performed using the Galaxy server (Afgan et al., 2018) and the "16S Microbial Analysis with Mothur" protocol (Hiltemann et al., 2019) with the modifications described by Dasi (2022). After clustering similar sequences into operational taxonomic units (OTUs), the data were downloaded from the Galaxy server for additional organizing and visualization. Note that each OTU is intended to represent a taxonomic group of bacteria (e.g., *Thiobacillus*) that was identified in a sample.

In-house Perl scripts were used to calculate each sample's average OTU percent abundance and OTU change over time. Changes in microbial community structure were expressed as fold change, which was calculated as the average OTU percent abundance at the final time over the abundance at the initial time. Calculated values used to visualize the microbial community composition and change are available in Dasi et al. (2023). Two figure types were created using RStudio® (version 1.2.5042) (R Core Team, 2020): (1) stacked bar charts showing the relative microbial community composition, and (2) bar charts depicting the microbial community change by a factor of two (i.e., $\log_2$ fold change). Note that some OTUs were undetected (i.e., 0%) in a sample at the initial or final time points. For these, $\log_2$ fold change values could not be calculated, and the OTU was described as either "appeared" or "disappeared." Uncharacterized OTUs to at least the order level were combined by taxonomic rank to represent phylum_unclassified and class_unclassified for both figure types. In addition, the term "unclassified" was removed from OTUs only classified to the order and family ranks. Unknown OTUs are characterized as bacteria_unclassified in the figures and Dasi et al. (2023).

2.6 Data analysis

Average denitrification rates were estimated by Equation 1, using the final and initial NO_3^--N concentrations.

$$\text{Average denitrification rate } \left(\frac{\text{mg}}{\text{L} \cdot \text{d}}\right) = \frac{C_i - C_f}{t_f - t_i} \quad (1)$$

where C and t denote the NO_3^- concentration (mg N/L) and time (d), respectively.

Total organic nitrogen (TON) concentration was calculated by subtracting the total inorganic nitrogen (TIN = NO_3^--N + NO_2^--N + NH_4^+-N) from the TN concentration. Total organic phosphorus (TOP) concentration was estimated calculated by subtracting the PO_4^{3-}-P concentration from the TP concentration.

Theoretical S/N ratios (i.e., SO_4^{2-}produced/NO_3^--N consumed) were estimated for S^0 (Equation 2, Batchelor and Lawrence, 1978) and sphalerite (Equations 3 and 4) autotrophic denitrification. Equations 3 and 4 were developed for the two different sphalerite sources using the method of McCarty (1975), thermodynamic data from Lide (1991) and Tagirov and Seward (2010), and assuming empirical formulas for sphalerite, based on the X-ray diffraction patterns (Dasi, 2022).

$$1.10\ S^0 + 0.40\ CO_2 + NO_3^- + 0.76\ H_2O + 0.08\ NH_4^+ \Rightarrow$$
$$0.08\ C_5H_7O_2N + 0.50\ N_2 + 1.10\ SO_4^{2-} + 1.28\ H^+ \quad (2)$$

$$0.746\ Zn_{0.628}Fe_{0.372}S + 0.250\ CO_2 + NO_3^- + 1.19\ H_2O + 0.0625\ NH_4^+ + 0.0625\ HCO_3^- \Rightarrow$$
$$0.468\ Zn(OH)_2 + 0.278\ Fe(OH)_3 + 0.0625\ C_5H_7O_2N + 0.50\ N_2 + 0.746\ SO_4^{2-} + 0.493\ H^+ \quad (3)$$

$$0.764\ Zn_{0.825}Fe_{0.175}S + 0.250\ CO_2 + NO_3^- + 1.159\ H_2O + 0.0625\ NH_4^+ + 0.0625\ HCO_3^- \Rightarrow$$
$$0.631\ Zn(OH)_2 + 0.134\ Fe(OH)_3 + 0.0625\ C_5H_7O_2N + 0.50\ N_2 + 0.764\ SO_4^{2-} + 0.529\ H^+ \quad (4)$$

Statistical testing was performed using the Origin 9 software (OriginLab, 2021). Replicates were examined to determine whether a sample was well-modeled by a normal distribution using the Anderson-Darling test (Anderson and Darling, 1952). Those samples with replicates that followed a normal distribution were tested using parametric statistics. One-way ANOVA testing was applied to compare three or more independent samples. Alternatively, two sample t-testing was used to compare fewer than three independent samples. Results from the one-way ANOVA testing were only considered for samples that had equal variance with the Brown-Forsythe test (Brown and Forsythe, 1974). The Welch t-statistic was considered during two sample t-testing for comparisons with unequal variance (Welch, 1947). Comparisons with *p* values less than 0.05 were considered significantly different.

3. Results and discussion

3.1 Denitrification performance of sphalerite, with and without oyster shells

3.1.1 N removal

Figure 1 shows the N species concentration profiles for Phases 1 and 2. NO_3^- reduction in the controls was generally as anticipated. NO_3^- was undetected in the S^0 + OS positive control by day 13 (Fig. 1A), demonstrating that the methodology applied was sufficient to support autotrophic denitrification. As a result, analysis of the denitrification performance beyond day 13 for the S^0 + OS batch reactors was discontinued. The NO_3^- concentration profile in the UN reactors was relatively stable, indicating that neither sphalerite nor OS directly reduced NO_3^- without a specialized microbial community (see supplementary materials). NO_3^- removal in the inoculum-only control was higher than expected (Fig. 1A and 1B), indicating that particulate organic matter in the inoculum or endogenous decay of the inoculum provided substrate for heterotrophic denitrification in the biotic reactors.

Gradual NO_3^- removal was observed in the batch reactors with sphalerite (Fig. 1A and 1B). Initially, NO_3^- concentrations in the sphalerite and inoculum-only reactors tracked closely, suggesting the heterotrophic denitrification might have been the main NO_3^- removal mechanism at early times. However, mean NO_3^- concentrations of the sphalerite reactors remained significantly different than the inoculum-only control after days 34 and 13 of Phase 1 and Phase 2, respectively ($p < 0.030$; see supplementary materials). These results indicate that although heterotrophic denitrification initially drove NO_3^- reduction in the batch reactors with sphalerite, mineral addition eventually increased NO_3^- removal. NO_3^- removal was also accompanied by NH_4^+ release during both phases (Fig. 1E and 1F), which might be due to dissimilatory nitrate reduction to ammonium (DNRA). This is discussed in more detail below.

Average denitrification rates and S/N ratios for Phases 1 and 2 can be found in the supplementary materials. Although the NO_3^- removal rate for the batch reactors with sphalerite was slower than the S^0 + OS control (Fig. 1A and 1B), the average denitrification rates for the reactors with sphalerite (1.0 mg/L*d) and sphalerite + OS (1.14 mg/L*d) were close to those observed by Li et al. (2022), who performed similar batch studies with pyrite (~ 1.1 mg/L*d). The use of solid-phase electron donors, such as sphalerite and pyrite, with suspended biomass in batch reactors may contribute to slow average denitrification rates. Application of these minerals in biofilm systems (e.g., packed-bed reactors) may improve their utilization by autotrophic denitrifying bacteria.

Mineral and OS addition improved N removal compared to using sphalerite as a substrate. As discussed previously, a slightly higher average denitrification rate was observed for the sphalerite + OS reactors than those with only sphalerite. TIN removal was also higher in the sphalerite + OS reactors over 67 days than those with mineral (70% vs. 60%; Fig. 1), suggesting that more NO_3^- was reduced to gaseous products. This likely occurred because NO_2^-

accumulation was lower in the sphalerite + OS batch reactors (Fig. 1C and 1D). NO_2^- accumulation possibly occurred since the NO_3^- reductase enzyme (Nar) preferentially accepts electrons over the enzyme responsible for NO_2^- reduction (i.e., Nir). As a result, NO_3^- reduction is prioritized and NO_2^- reduction delayed during denitrification (Richardson et al., 2009; Ucar et al., 2021). The high initial NO_3^- concentration of the prepared groundwater may have also inhibited the activity of the Nir enzyme, causing NO_2^- to accumulate (Fig. 1A and 1B; Glass and Silverstein, 1998). Colonization of a unique consortium of bacteria on the sphalerite + OS reactor media may have supported better N removal than the sphalerite reactors. Key microbial drivers involved in transforming N are discussed further in Section 3.3.3.

3.1.2 SO_4^{2-} By-product Formation

Figure 2 shows additional chemical results for Phases 1 and 2. Day 0 SO_4^{2-} concentrations for the reactors with sphalerite were similar to the inoculum-only control (Fig. 2A and 2B). This suggested that mineral preparation did not cause substantial surface sulfide oxidation, which could increase aqueous SO_4^{2-} concentration in the reactors. As expected, SO_4^{2-} production was only observed in the reactors containing either S^0 or sphalerite (Fig. 2A and 2B). SO_4^{2-} in the S^0 + OS positive control was below the maximum theoretical concentration (~860 mg/L) based on Equation (2), but sufficiently high to confirm that autotrophic denitrification occurred (Fig. 2A). In contrast, much lower and gradual SO_4^{2-} production was observed in the batch reactors with sphalerite (Fig. 2A and 2B). Sphalerite oxidation is described to occur in a two-step process. During the first step, sulfide is incompletely oxidized to S^0 to form a layer on the mineral surface. Bacterial oxidation of this layer can proceed afterward, leading to the production of SO_4^{2-} (Fowler and Crundwell, 1999; Zapata et al., 2007). Heterotrophic denitrification and incomplete sulfide oxidation may have occurred simultaneously as S autotrophic bacteria were cultivated in the batch reactors with sphalerite. This might explain why the observed S/N ratios for sphalerite-

driven denitrification in Phase 1 (1.50 mg SO_4^{2-}/mg NO_3^-) and Phase 2 (1.58 mg SO_4^{2-}/mg NO_3^-) were below the theoretical value (5.1 mg SO_4^{2-}/mg NO_3^-) obtained from Equation (3). The peroxide method applied by Pu et al. (2014) could be used in future research to quantify incomplete S oxidation when sphalerite is used for autotrophic or mixotrophic denitrification.

3.1.3 P Removal

Clear P removal occurred in the batch reactors containing sphalerite (Fig. 2C and 2D). PO_4^{3-} removal was also observed in the sphalerite UN batch reactor (see supplementary materials), suggesting that abiotic processes (i.e., precipitation and adsorption) may play a role. Yang et al. (2017) found that precipitates, such as $FePO_4$ and $Fe(OH)_3$, were likely responsible for P adsorption onto pyrrhotite in anoxic packed-bed reactors. Mineral surface chemistry was not evaluated in Phases 1-3. However, sphalerite autotrophic denitrification may drive P removal mechanisms that are similar to those described by Yang et al. (2017) and involve iron and zinc (Almasri et al., 2021). PO_4^{3-} was completely removed from the sphalerite + OS reactors in approximately half the time observed for its mineral-only counterpart (Fig. 2C and 2D). OS addition most likely supported additional precipitation processes, as it contains approximately 97% calcium carbonate (Asaoka et al., 2009). Calcium released from the OS possibly precipitated with PO_4^{3-} to form hydroxyapatite ($Ca_{10}(PO_4)_6OH_2$), which could have been adsorbed onto sphalerite's surface (Khan et al., 2020).

3.2 Effect of sphalerite and oyster shells dose on denitrification performance

Phase 3 further confirms that sphalerite can be used as an electron donor for autotrophic denitrification. Figures 3 and 4 show the results obtained for this phase. Simultaneous NO_3^- removal and SO_4^{2-} production were observed during each cycle, confirming that S oxidation occurred concurrently with denitrification in the sphalerite + OS reactor (Fig. 3A and 3B). Close

347 tracking of the sphalerite + OS reactor's observed SO_4^- concentration profile with the theoretical
348 trend provides additional evidence of S autotrophic denitrification (Fig. 3B).
349 Mixotrophic denitrification during cycle 1 may explain the observed trends in the
350 sphalerite + OS batch reactor. Slight NO_3^- reduction and NO_2^- production were observed in the
351 inoculum-only control during cycle 1, suggesting that heterotrophic denitrification initially
352 occurred in the sphalerite + OS reactors (Fig. 3A and 3C). COD, TON, and TOP were also
353 removed from the sphalerite + OS reactor during cycle 1, which provides additional evidence of
354 heterotrophic denitrification (Fig. 4A - 4C). Based on the COD consumed and the stoichiometric
355 requirements for heterotrophic denitrification (2.86 mg COD/mg NO_3^--N; Ergas and Aponte-
356 Morales, 2014), only 4.2 mg/L NO_3^--N could have been removed by this mechanism (~ 40 mg/L
357 NO_3^--N were removed in cycle 1; Fig. 3A). Concurrent heterotrophic and autotrophic
358 denitrification during cycle 1 in the sphalerite + OS reactor may explain the observed alkalinity
359 production (Fig. 4D) and higher average denitrification rates compared to the subsequent cycles
360 (Fig. 3A). Similar SO_4^- concentration profiles between the observed and theoretical trends for the
361 sphalerite + OS reactors suggest that that heterotrophic denitrification became negligible over
362 time (Fig. 3B).
363 Results from cycles 2 and 3 suggest that increasing sphalerite and OS dose may not
364 improve NO_3^- removal. Average denitrification rates between cycles 2 and 3 declined in the
365 sphalerite + OS batch reactor (Fig. 3A). Prior research suggests that layers formed on sphalerite's
366 surface can block the diffusion of soluble substrates to autotrophic bacteria, limiting the
367 denitrification rate (Fowler and Crundwell, 1999). PO_4^{3-} removal efficiency was maintained at
368 approximately 97% during cycles 1-3 (Fig. 3E), which suggests that precipitates responsible for P
369 removal accumulated on the mineral surface. These precipitates may have limited access of
370 sulfide to denitrifying bacteria, causing the average denitrification rate to decrease each cycle.

3.2 N-transformations and removal mechanisms of sphalerite autotrophic denitrification

3.3.1 Assessment of the microbial community analysis

Information of the 16S rRNA gene libraries obtained from the Illumina-based sequencing can be found in the supplementary material. Moderate percentages of effective sequences were recovered after quality filtering of the samples. Despite this, high Good's coverage values suggest that the microbial composition for each sample is well represented by the constructed sequence libraries and thus reflects the real bacterial profile. Examination of the 16S rRNA sequence libraries indicates that the data is of sufficient quality to investigate the microbial community composition and change.

3.3.2 Microbial community of the inoculum from a full-scale five-stage Bardenpho process

The inoculum contained a diverse consortium of bacteria, which possibly supports the removal of N, P, and organics at the NWRWRF. The supplementary material shows the microbial community composition of the initial inoculum. Dominant bacteria are considered as those representing more than 0.99% of the total population. Dominant bacteria in the inoculum included *Actinomycetales* (7.0%), *Intrasporangiaceae* (6.6%), *Planctomycetaceae* (3.8%), *Aquihabitans* (2.1%), *Conexibacter* (1.8%), and *Nitrospira* (1.7%) (see supplementary materials). Phosphate accumulating organisms (PAOs) belonging to *Intrasporangiaceae* may drive enhanced biological P removal at the NWRWRF (Lee and Park, 2008), while members of *Nitrospira* likely carry out nitrification (Dueholm et al., 2022). *Aquihabitans*, *Conexibacter*, *Actinomycetales,* and *Planctomycetaceae* might also contribute to the removal of organics through the conversion of NO_3^- to NO_2^- (Dueholm et al., 2022). Taxonomic groups with species that perform complete denitrification, such as *Defluviimonas* (0.34%) and *Paracoccus* (0.11%), were also detected in

393 the inoculum (Dasi et al., 2023; Dueholm et al., 2022). It is possible that bacteria belonging to
394 these genera convert NO_3^- or N intermediates of denitrification to $N_2(g)$ at the facility.

395 *3.3.3 Contribution of the microbial community to transforming N*

396 A synergy was observed between the microbial community and the chemistry of the
397 reactors. Figure 5 quantifies the microbial community change, considering the inoculum and
398 reactors of Phases 1 and 2. Table 2 also presents notable taxonomic groups identified during
399 these phases. Log_2 fold change values of *Intrasporangiaceae* ranged from -1.673 to -6.645 during
400 both phases, indicating that this taxonomic group decreased between 3 and 100-fold (i.e., 3 and
401 100 times) for each sample (Fig. 5A and 5B). Low bioavailable organic carbon in the reactors
402 may have resulted in volatile fatty acids concentrations below the requirements to sustain PAOs
403 of *Intrasporangiaceae*. This hypothesis is supported by the decline of *Trichococcus* (log_2 fold
404 change < -1.442; Fig. 5A and 5B), which include species that produce propionic acid by
405 fermentation (Dueholm et al., 2022). Conversely, *Ignavibacterium* emerged as a notable genus,
406 increasing in all samples at least four-fold (log_2 fold change > 2.135; Fig. 5A and 5B). Only one
407 species to date has been identified for *Ignavibacterium*, which contains a NrfAH complex that
408 converts NO_2^- to NH_4^+ during dissimilatory nitrate reduction to ammonium (DNRA) (Liu et al.,
409 2012). The presence of this genus suggests that DNRA may have caused NH_4^+ to accumulate
410 during Phases 1 and 2 (Fig. 1E and 1F). The sphalerite reactors had the greatest abundance of
411 *Ignavibacterium* compared to the others in Phase 1 (Table 2), suggesting that sulfide from the
412 mineral may have increased DNRA (Brunet and Garcia-Gill, 1996).

413 Several other taxonomic groups emerged over time to represent noteworthy populations.
414 *Chromatiaceae* and *Chromatiales* grew during both phases, with the greatest change generally
415 occurring in the reactors with sphalerite (log_2 fold change = 0.043-4.310; Dasi et al. (2023) and

Fig. 5). *Thiobacillus* also appeared and generally increased over time in the reactors containing sphalerite (Table 2). S oxidizing bacteria belonging to *Chromatiaceae*, *Chromatiales*, and *Thiobacillus* might have performed denitrification in Phases 1 and 2 (Dueholm et al., 2022). These genera had a lower abundance in the inoculum-only control compared to the sphalerite reactors by day 74 (Table 2), suggesting that less N may have been removed by autotrophic denitrification. *Candidatus Brocadiaceae* and *Candidatus Kuenenia*¸ whose species perform anammox (Dueholm et al., 2022), also appeared during Phase 2 after 67 days in the reactors containing OS reactors (Table 2). The presence of *Candidatus Brocadiaceae* and *Candidatus Kuenenia* in the OS-only reactors suggests that OS might have cultivated these organisms. Combined sphalerite and OS addition supported the growth of anammox, S autotrophic denitrifying, and DNRA bacteria, which likely coordinated to drive NO_3^- removal (Fig. 1B) while maintaining a low NO_2^- concentration profile (Fig. 1D). Bacterial competition in the sphalerite + OS reactors may explain the lower abundance of autotrophic denitrifying bacteria and DNRA bacteria than those with mineral (Table 2).

3.3.4 Mechanisms of N removal during sphalerite autotrophic denitrification

Figure 6 shows the microbial community structure that formed in reactor with sphalerite, OS, and domestic wastewater on day 140. Interestingly, many of the bacteria representing more than 2% of the population belong to the phylum *Proteobacteria*. This taxonomic group is metabolically diverse, containing phototrophic, chemoheterotrophic, and chemoautotrophic bacteria (Dueholm et al., 2022). Notable taxonomic groups of *Proteobacteria* included *Chromatiales* (2.4%) and *Burkholderiales* (1.1%) (Fig. 6). Like *Chromatiales*, some species of *Burkholderiales* couple S oxidation with NO_3^- reduction or complete denitrification (Dueholm et al., 2022). The presence of these orders may suggest their involvement in removing N in the

sphalerite + OS batch reactor of Phase 3. Research indicates that the microbial community structure during S autotrophic denitrification is dependent on the electron donor provided (Zhou et al., 2017). The identification of *Chromatiales* in Phases 1-3 may suggest that S autotrophic bacteria belonging to this order are possibly linked to driving sphalerite autotrophic denitrification (Table 2).

3.4 Implications and potential limitations

Based on the results, sphalerite autotrophic denitrification could be considered for future water management strategies to address nutrient pollution. The cost of sphalerite is comparable to pyrite (~ $2.30/kg; IGF, 2023). However, slower denitrification rates were observed compared with other metal sulfide minerals (Dasi, 2022) and secondary pollution of trace metals (e.g., zinc) released following S oxidation may limit the application of sphalerite autotrophic denitrification. Designs that can maintain long hydraulic residence times, such as horizontal subsurface flow constructed wetlands, might be suitable to harness sphalerite autotrophic denitrification for nutrient control, as has been done previously with pyrite (Ge et al., 2019). Future research should explore strategies to improve denitrification rates and clarify trace metal effluent quality during sphalerite autotrophic denitrification. Other areas worth exploring involve uncovering specific mechanisms of PO_4^{3-} removal and quantifying potential greenhouse gas emissions by measuring nitrous oxide production during sphalerite-driven denitrification.

4. Conclusions

This is the first study to evaluate sphalerite as an electron donor for autotrophic denitrification. Sphalerite promoted NO_3^- and PO_4^{3-} removal from groundwater. Mineral and OS addition minimized NO_2^- accumulation and promoted faster PO_4^{3-} removal than sphalerite alone. Increasing sphalerite and OS dose did not improve domestic wastewater denitrification; however,

462 long-term NO_3^- and PO_4^{3-} removal (140 d) was supported. 16S rRNA amplicon sequencing
463 suggests that S oxidizing species of *Chromatiales*, *Burkholderiale*s, and *Thiobacillus* drive N
464 removal during sphalerite autotrophic denitrification. These results provide an improved
465 understanding of S autotrophic denitrification, which can be refined to develop solutions for
466 nutrient control.

467 **5. Appendix A: Supplementary materials**

468 E-supplementary data for this work can be found in the online version of the paper.

469 **6. Acknowledgements**

470 This research work was supported by the USEPA (Grant No. RD 83560201-0), National
471 Science Foundation (Grant Nos. 1243510 and 1735320), Alfred P. Sloan Foundation (Grant No.
472 2017-9717), Chateaubriand Fellowship Program, Florida Education Fund, and USF's Institute for
473 Microbiomes. The LCB laboratory was funded by CNRS and Aix Marseille University.

474 **References**

475 1. Afgan, E., Baker, D., Batut, B., van den Beek, M., Bouvier, D., Čech, M., Chilton, J.,
476 Clements, D., Coraor, N., Grüning, B., Guerler, A., Hillman-Jackson, J., Jalili, V., Rasche,
477 H., Soranzo, N., Goecks, J., Taylor, J., Nekrutenko, A., Blankenberg., D., 2018. The Galaxy
478 platform for accessible, reproducible and collaborative biomedical analyses: 2018 update.
479 Nucleic Acids Res., 46(W1), W537-W544.
480 2. Almasri, D.A., Essehli, R., Tong, Y., Lawler, J., 2021. Layered zinc hydroxide as an
481 adsorbent for phosphate removal and recovery from wastewater. RSC Adv., 11, 30172-
482 30182.
483 3. Anderson, T.W., Darling, D.A., 1952. Asymptotic Theory of Certain "Goodness of Fit"
484 Criteria Based on Stochastic Processes. Ann. Math. Statist. 23(2), 193-212.

4. Anthony, J.W., Bideaux, R.A., Bladh, K.W., Nichols, M.C., 1990. Handbook of Minerology. Mineralogical Society of America, Chantilly, VA, USA.
5. APHA, AWWA, WEF, 2017. Standard Methods for the Examination of Water & Wastewater. 23rd Edition. American Public Health Association, American Water Works Association, and Water Environment Federation. Washington, D.C., USA
6. Asaoka, S., Yamamoto, T., Kondo, S., Shinjiro, H., 2009. Removal of hydrogen sulfide using crushed oyster shell from pore water to remediate organically enriched coastal marine sediments. Bioresour. Technol., 100(18), 4127-4132.
7. Batchelor, B., Lawrence, A.W., 1978. Autotrophic denitrification using elemental sulfur. J. Water Pollut. Control Fed., 50(8), 1986-2001.
8. Brown, M.B., Forsythe, A.B., 1974. Robust Tests for the Equality of Variances, J. Am. Stat. Assoc. 69(346), 364-367.
9. Brunet, R.C., Garcia-Gil, L.J., 1996. Sulfide-induced dissimilatory nitrate reduction to ammonia in anaerobic freshwater sediments. Fems Microbiol. Ecol. 21(2), 131-138.
10. Dasi, E.A., 2022. Elemental Sulfur and Metal Sulfide Minerals for Autotrophic Denitrification: Applications to Aquaculture, Groundwater Treatment, and Domestic Wastewater Treatment. USF Tampa Graduate Theses and Dissertations.
11. Dasi, E.A., Cunningham, J.A., Talla, E., Ergas, S.J., 2023. Microbial community dataset for sphalerite and oyster shell denitrification study, Mendeley Data, V2, doi: 10.17632/h696jj4pf8.1
12. Dueholm, M. K. D., Nierychlo, M., Andersen, K.S., Rudkjøbing, V., Knutsson, S., Albertsen, M., Nielsen, P.H., 2022. MiDAS 4: A global catalogue of full-length 16S rRNA gene sequences and taxonomy for studies of bacterial communities in wastewater treatment plants. Nat. Commun. 13(1908), 1-15.

13. Ergas, S.J., Reuss, A. (2001) Hydrogenotrophic denitrification of drinking water using a hollow fiber membrane bioreactor, J. Water Supply Res. T., 50(3):161-171.
14. Ergas, S.J, Aponte-Morales, V., 2014. Biological Nurtient Removal. In: Ahuja, S. (Ed.) Comprehensive Water Quality and Purification. Elsevier Inc. Amsterdam, Netherlands.
15. Fowler, T.A., Crundwell, F.K., 1999. Leaching of zinc sulfide by Thiobacillus ferroxidans: Bacterial oxidation of the sulfur product layer increases the rate of zinc sulfide dissolution at high concentrations of ferrous iron. Appl. Environ. Microbiol., 65(12), 5285-5292.
16. Gasteyer, S., 2010. Are small community water systems more at risk than other systems? https://www.yumpu.com/en/document/read/24194396/are-small-community-water-systems-more-at-risk-than-other-
17. Ge, Z., Wei, D., Zhang, J., Hu, J., Liu, Z., Li, R., 2019. Natural pyrite to enhance simultaneous long-term nitrogen and phosphorus removal in constructed wetland: three years of pilot study. Water Res., 148, 153-161.
18. He, Q., Dasi, E. A., Cheng, Z., Talla, E., Main, K., Feng, C., Ergas, S.J., 2021. Wood and sulfur-based cyclic denitrification filters for treatment of saline wastewaters. Bioresour. Technol. 328, 124848-124857.
19. Hiltemann, S., Batut, B., Clements, D., 2019. 16S Microbial Analysis with mothur (extended) (Galaxy Training Materials). /training-material/topics/metagenomics/tutorials/mothur-miseq-sop/tutorial.html Online
20. Hu, Y., Wu, G., Li, R., Xiao, L., Zhan, X., 2020. Iron sulphides mediated autotrophic denitrification: an emerging bioprocess for nitrate pollution mitigation and sustainable wastewater treatment. Water Res., 179, 115914-115939.
21. Intergovernmental Forum on Mining, Minerals, Metals and Sustainable Development (IGF), 2023. Mineral pricing. https://www.igfmining.org/beps/current-topics/mineral-pricing/

22. Khan, M.D., Chottitisupawong, T., Hong, Vu, H.H.T., Ahn, J.W., Kim, G.M., 2020. Removal of phosphorus from an aqueous solution by nanocalcium hydroxide derived from waste bivalve seashells: mechanism and kinetics. ACS Omega., 5, 21, 12290-12301.

23. Kong, Z., Li, L., Feng, C., Dong, S., Chen, N., 2016. Comparative investigation on integrated vertical-flow biofilters applying sulfur-based and pyrite-based autotrophic denitrification for domestic wastewater treatment. Bioresour. Technol., 211, 125-135.

24. Lee, H.W. and Park, Y.K., 2008. Characterizations of denitrifying polyphosphate-accumulating bacterium *Paracoccus* sp. strain YKP-9. J. Microbiol. Biotechnol., 18(12), 1958-1965

25. Li, R.H., Niu, J.M., Zhan, X.M., 2013. Simultaneous removal of nitrogen and phosphorus from wastewater by means of FeS-based autotrophic denitrification. Water Sci. Technol., 67(12), 2761-2767.

26. Li, R., Morrison, L., Collins, G., Li, A., Zhan, X., 2016. Simultaneous nitrate and phosphate removal from wastewater lacking organic matter through microbial oxidation of pyrrhotite coupled to nitrate reduction. Water Res., 96, 32-41.

27. Li, R., Zhang, Y., Guan, M., 2022. Investigation into pyrite autotrophic denitrification with different mineral properties. Water Res., 221, 118763-118771.

28. Lide, D.R., 1991. CRC Handbook of Chemistry and Physics. 71st edition. CRC Press, Boca Raton, FL, USA

29. Liu, Z., Frigaard, N. U., Vogl, K., Iino, T., Ohkuma, M., Overmann, J., Bryant, D. A., 2012. Complete Genome of Ignavibacterium album, a Metabolically Versatile, Flagellated, Facultative Anaerobe from the Phylum Chlorobi. Front. Microbiol., 3, 1-15.

30. McCarty, P.L., (1975) Stoichiometry of biological reactions. Prog. Water Technol. 7, 157-172.

31. OriginLab Corporation, 2021. OriginPro®, Northampton, MA, USA.
32. Oxenford, J. L., Barrett, J. M., 2016. Understanding small water system violations and deficiencies. J. Am. Water Works Assoc., 108(3), 31-37.
33. Park, W.H, Polprasert, C., 2008. Phosphorus adsorption characteristics of oyster shells and alum sludge and their application for nutrient control in constructed wetland system. J. Environ. Sci. Health A Tox. Hazard Subst. Environ. Eng., 43(5), 511–517.
34. Pu, J., Feng, C., Liu, Y., Kong, Z., Chen, N., Tong, S., Hao, C., Liu, Y., 2014. Pyrite-based autotrophic denitrification for remediation of nitrate contaminated groundwater. Bioresour. Technol., 173, 117-123.
35. R Core Team (2020). R: A language and environment for statistical computing. R Foundation for Statistical Computing, Vienna, Austria. URL https://www.R-project.org/.
36. Richardson, D., Felgate, H., Watmough, N., Thomson, A., Baggs, E., 2009. Mitigating release of the potent greenhouse gas N_2O from the nitrogen cycle - could enzymatic regulation hold the key? Trends Biotechnol., 27(7), 388-397.
37. Sengupta, S., Ergas, S.J., Lopez-Luna, E., 2007. Investigation of solid-phase buffers for sulfur-oxidizing autotrophic denitrification. Water Environ Res., 79(13), 2519-2526.
38. Shih, J.S., Harrington, W., Pizer, W.A., Gillingham, K., 2006. Economies of scale in community water systems. J. Am. Water Works Ass., 98(9), 100-108.
39. Sierra-Alvarez, R., Beristain-Cardoso, R., Salazar, M., Gomez, J., Razo-Flores, E., Field, J.A., 2007. Chemolithotrophic denitrification with elemental sulfur for groundwater treatment. Water Res., 41(6), 1253-1262.
40. Tagirov, B.R., Seward, T.M., 2010. Hydrosulfide/sulfide complexes of zinc to 250 °C and the thermodynamic properties of sphalerite. Chem. Geol., 269(3-4), 301-311.

41. Tong S., Stocks, J.L., Rodriguez-Gonzalez, L.C., Feng, C., Ergas, S.J., 2017. Effect of oyster shell medium and organic substrate on the performance of a particulate pyrite autotrophic denitrification (PPAD) process. Bioresour. Technol., 244, 296-303.

42. Tong, S., Rodriguez-Gonzalez, L.C., Payne, K.A., Stocks, J.L., Feng, C., Ergas, S.J., 2018. Effect of pyrite Pretreatment, particle size, Dose, and biomass concentration on particulate pyrite autotrophic denitrification of nitrified domestic wastewater. Environ. Eng. Sci., 35(8), 875-886.

43. Ucar, D., Di Capua, F., Yücel, A., Nacar, T., Sahinkaya, E., 2001. Effect of nitrogen loading on denitrification and filtration performances of membrane bioreactors fed biogenic and chemical elemental sulfur. J. Chem. Eng., 419, 129514-129524.

44. Ward, M.H., Jones, R.R., Brender, J.D., de Kok, T.M., Weyer, P.J., Nolan, B.T., Villanueva, C.M., van Breda, S.G., (2018). Drinking water nitrate and human health: an updated review. Int. J. Environ. Res. Publ. Health, 15, 1557-1588.

45. Welch, B.L., 1947. The generalisation of students' problem when several different population variances are involved. Biometrika. 34(1-2):28-35.

46. Yang, Y., Chen, T., Morrison, L., Gerrity, S., Collins, G., Porca, E., Li, R., Zhan, X., 2017. Nanostructured pyrrhotite supports autotrophic denitrification for simultaneous nitrogen and phosphorus removal from secondary effluents. Chem. Eng. J., 328(15), 511-518.

47. Zapata, D.M., Márquez, M.A., Ossa, D.M., 2007. Sulfur product layer in sphalerite biooxidation: Evidence for a mechanism of formation. Adv. Mat. Res., 20-21, 134-138.

48. Zhou, W., Li, Y., Liu, X., He, S., Huang, J.C., 2017. Comparison of microbial communities in different sulfur-based autotrophic denitrification reactors. Appl. Microbiol. Biotechnol. 101, 447-453.

Figure Captions

Fig. 1. Phase 1 and 2 batch reactor N concentration profiles. (A, C, E) Phase 1. (B, D, F) Phase 2.

Fig. 2. Phase 1 and 2 batch reactor SO42- and PO43- concentration profiles. (A, C) Phase 1. (B, D) Phase 2.

Fig. 3. Phase 3 batch reactor chemical profiles. (A) Nitrate. (B) Sulfate. (C) Nitrite. (D) Ammonium. (E) Phosphate. The vertical lines indicate the beginning of another cycle, after half the reactors' liquid volume was replaced with fresh domestic wastewater. ADR = Average denitrification rate of the sphalerite + OS batch reactor expressed in mg/(L·d).

Fig. 4. Additional chemical measurements of the Sphalerite + OS batch reactor during Phase 3, cycle 1. (A) N profile. (B) P profile. (C) Chemical oxygen demand. (D) Alkalinity. (E) pH.

Fig. 5. Relative change in the microbial community composition between the batch reactors and initial inoculum. (A) Phase 1. (B) Phase 2. Bacteria representing ≥ 0.1% of the total reads and that have Log2 fold changes between -5.0 and 3.2 in at least one of the samples are shown.

Fig. 6. Relative abundance of bacteria in the Sphalerite + OS batch reactors of Phase 3. Most bacteria that are shown are ≥ 2% in abundance. Others is comprised of bacteria that are less than 2% of the total population. Bacteria with an asterisk mark are members of the phylum *Proteobacteria*.

635 Fig. 1
636

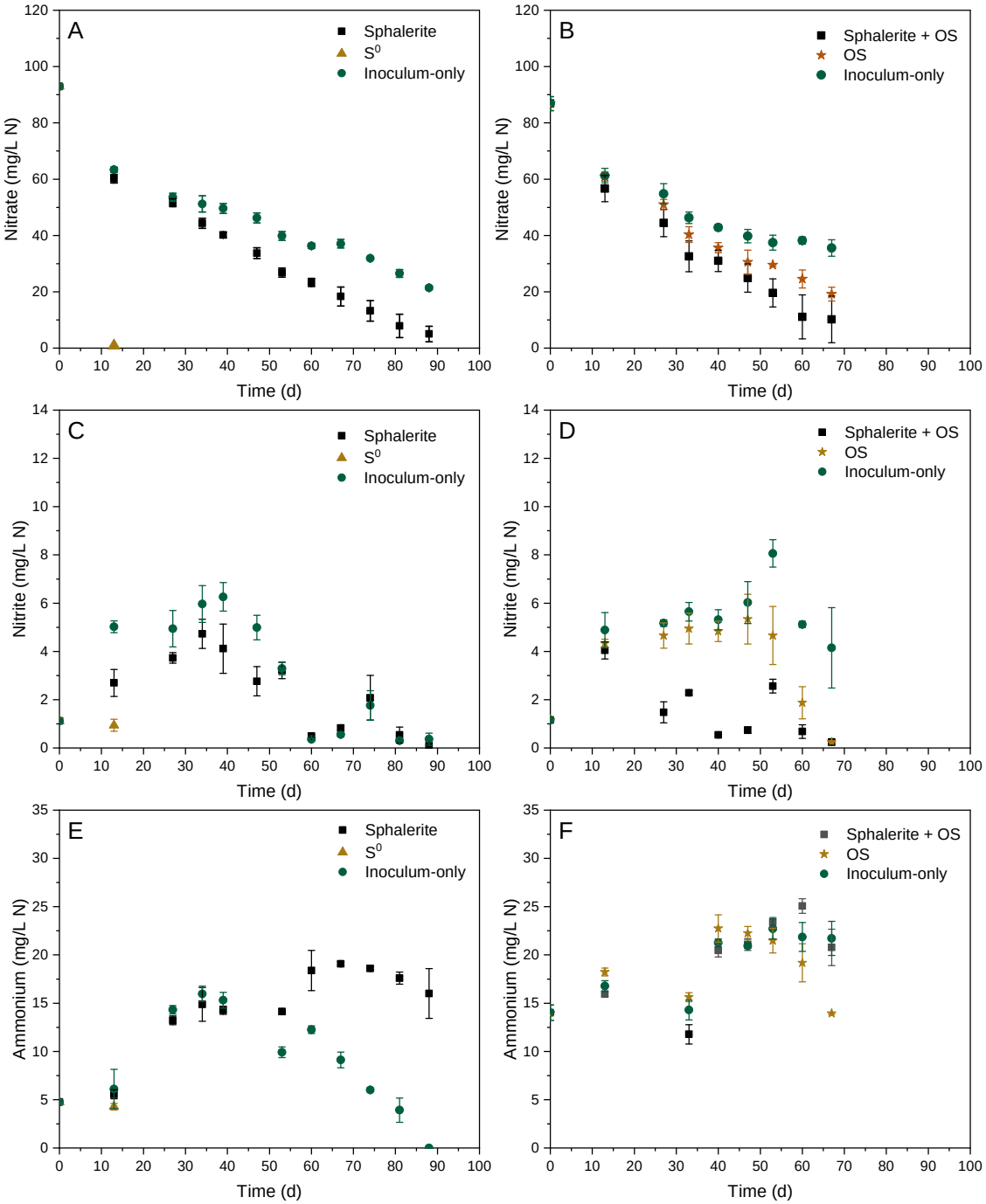

637
638
639
640

641 Fig. 2
642

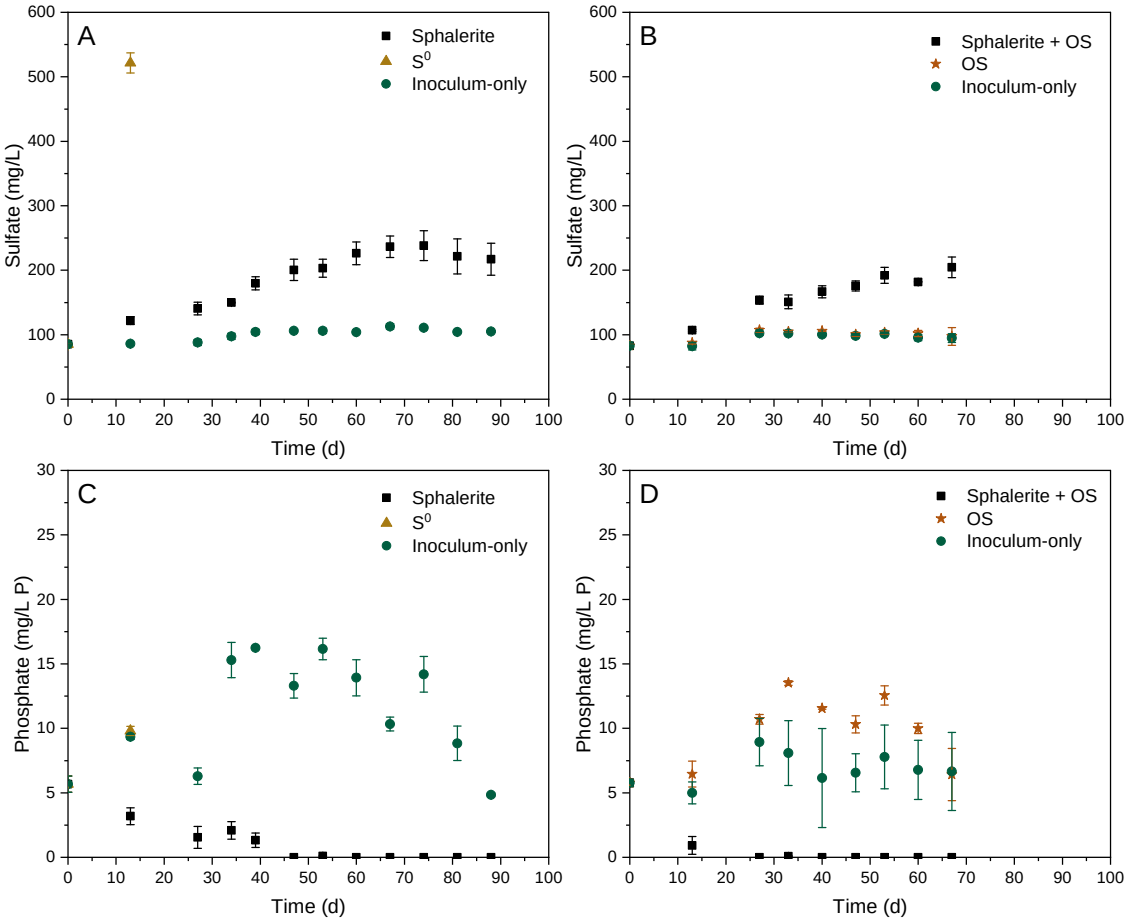

643
644
645
646
647
648
649
650
651
652
653
654
655
656
657
658
659
660

661 Fig. 3

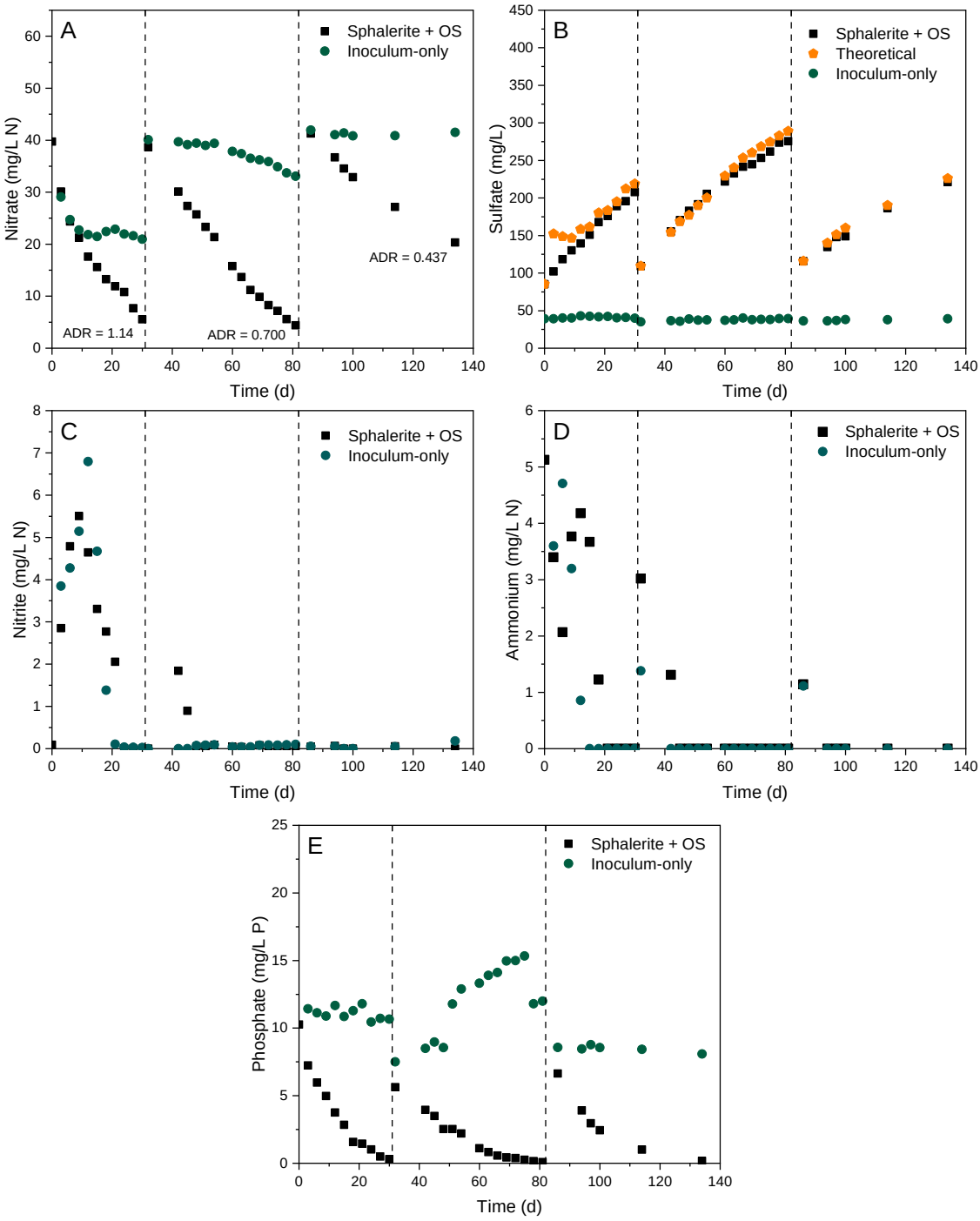
A
Sphalerite + OS
Inoculum-only
Nitrate (mg/L N)
ADR = 1.14
ADR = 0.700
ADR = 0.437
Time (d)
B
Sphalerite + OS
Theoretical
Inoculum-only
Sulfate (mg/L)
Time (d)
C
Sphalerite + OS
Inoculum-only
Nitrite (mg/L N)
Time (d)
D
Sphalerite + OS
Inoculum-only
Ammonium (mg/L N)
Time (d)
E
Sphalerite + OS
Inoculum-only
Phosphate (mg/L P)
Time (d)

662

663 Fig. 4

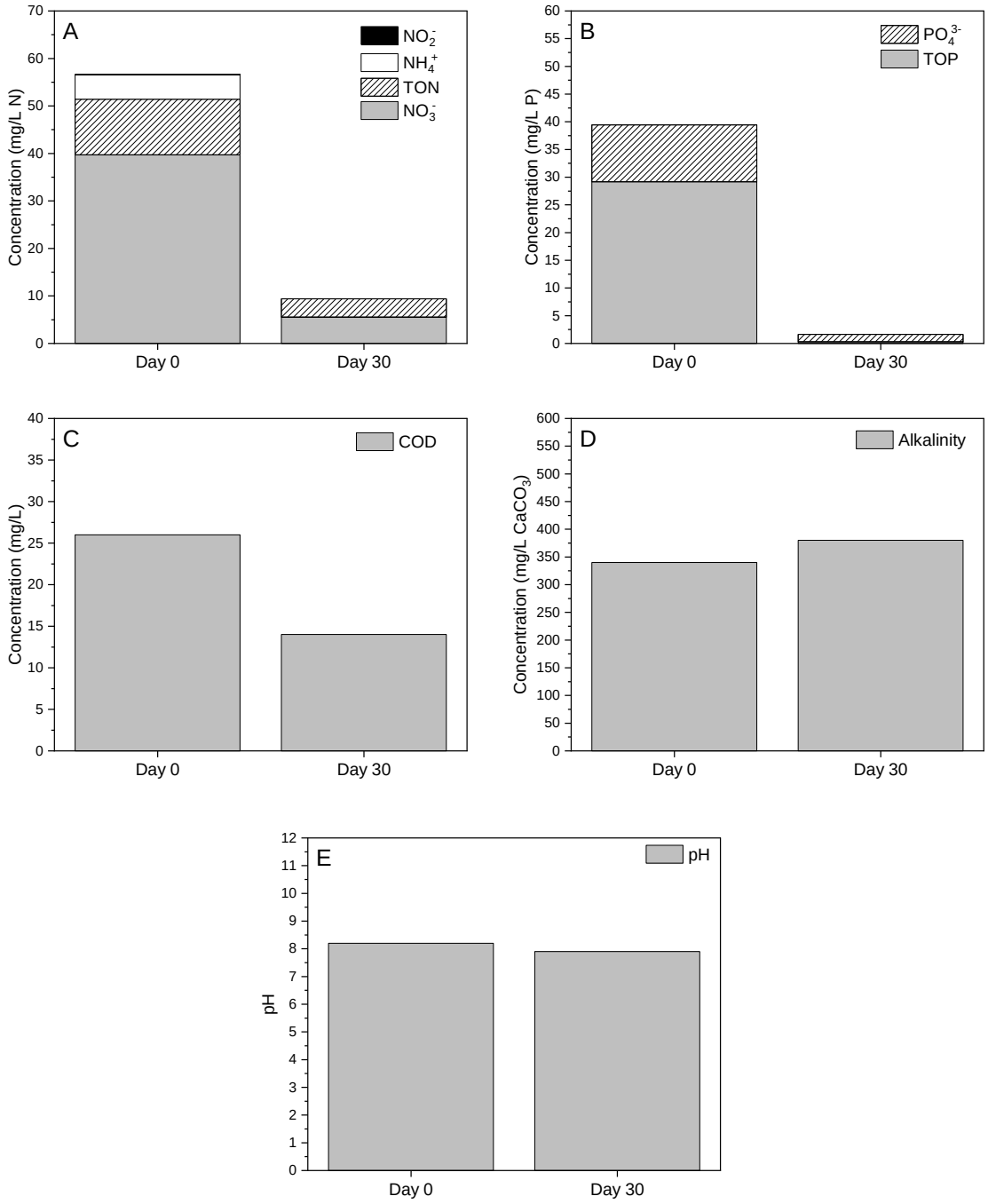

664
665

666 Fig. 5
667

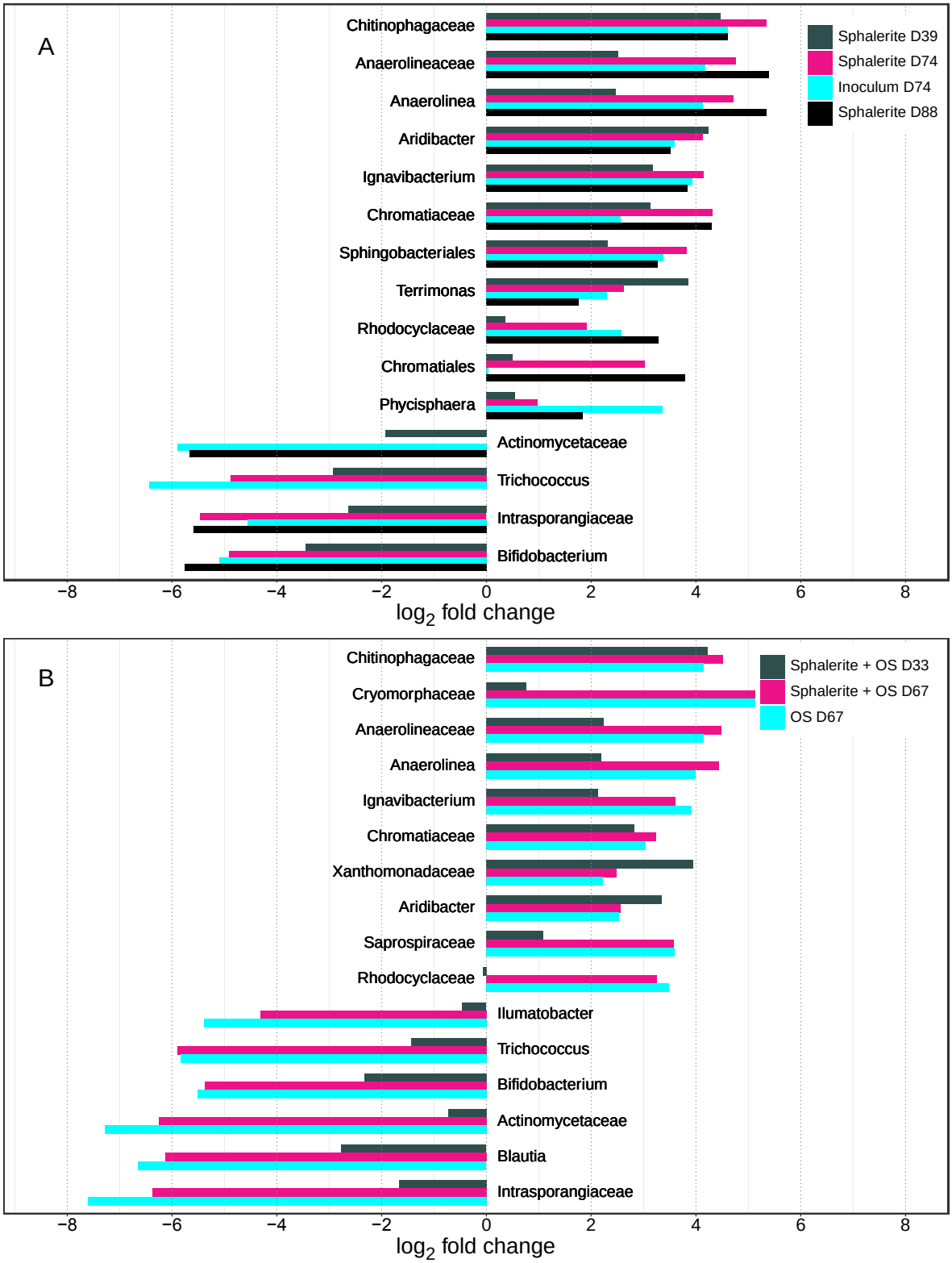

668
669

Fig. 6

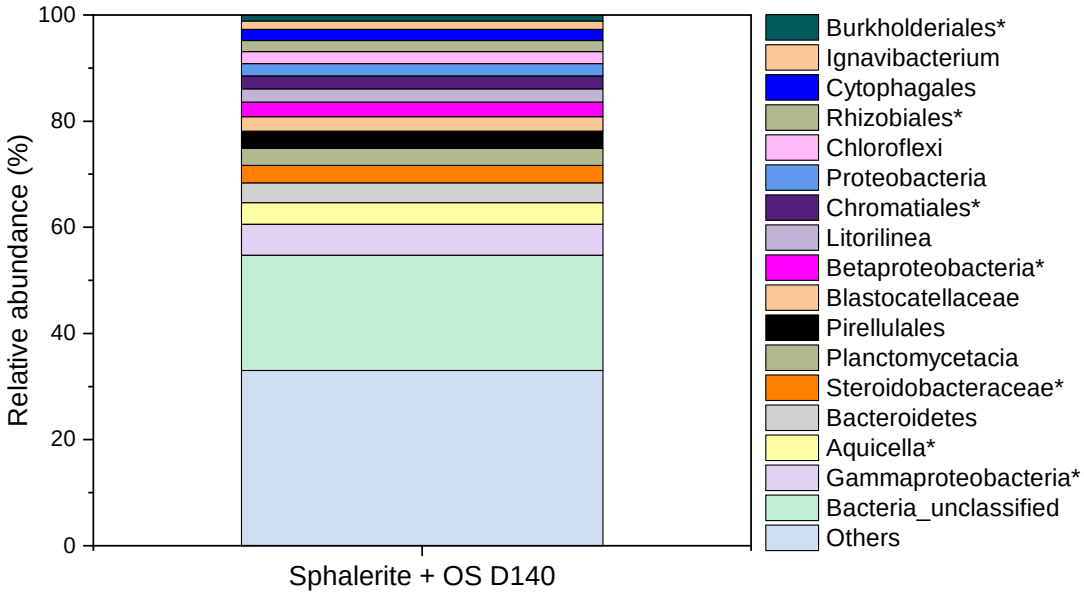
Relative abundance (%)
100
80
60
40
20
0
Sphalerite + OS D140
Burkholderiales*
Ignavibacterium
Cytophagales
Rhizobiales*
Chloroflexi
Proteobacteria
Chromatiales*
Litorilinea
Betaproteobacteria*
Blastocatellaceae
Pirellulales
Planctomycetacia
Steroidobacteraceae*
Bacteroidetes
Aquicella*
Gammaproteobacteria*
Bacteria_unclassified
Others

Table 1 Batch denitrification study details. Note: S^0 = Elemental Sulfur; OS = Oyster shells; UN = Uninoculated.

	Phase 1	Phase 2	Phase 3
Description**:**	Sphalerite-based autotrophic denitrification of groundwater	Effect of combined sphalerite & oyster shells on nutrient removal from groundwater	Effect of sphalerite & oyster shell dose on nutrient removal from domestic wastewater
Liquid volume (mL)	100	100	900
Duration (d)	88	67	140
Experimental Reactors	Sphalerite (12 g)	Sphalerite + OS (12 g; 4 g) OS (4 g)	Sphalerite + OS (Cycle 1: 164 g; 41 g) (Cycles 2 & 3: 258 g; 47 g)
Control Reactor(s)	Inoculum-only S^0 + OS (12 g + 4 g) Sphalerite UN (12 g)	Inoculum-only OS UN (4 g)	Inoculum-only
Sample collection for microbial community analysis	Days 0, 39, 74, 88	Days 0, 33, 67	Day 140

Table 2 Relative abundance of notable bacteria identified in Phase 1 and 2. UD = undetected.

Phase 1	*Chromatiaceae*	*Chromatiales*	*Thiobacillus*	*Candidatus Kueneia*	*Candidatus Brocadiaceae*	*Ignavibacterium*
Sphalerite D39	0.32%	0.044%	0.24%	UD	UD	1.6%
Sphalerite D74	0.71%	0.25%	0.19%	UD	UD	3.2%
Inoculum D74	0.21%	0.032%	0.003%	0.057%	UD	2.8%
Sphalerite D88	0.71%	0.43%	0.43%	0.054%	UD	2.6%
Phase 2	*Chromatiaceae*	*Chromatiales*	*Thiobacillus*	*Candidatus Kueneia*	*Candidatus Brocadiaceae*	*Ignavibacterium*
Sphalerite + OS D33	0.26%	0.055%	0.083%	UD	UD	0.80%
Sphalerite + OS D67	0.34%	0.036%	0.009%	0.35%	0.94%	2.2%
OS D67	0.25%	0.080%	0.007%	1.0%	0.14%	2.7%

Autotrophic denitrification supported by sphalerite and oyster shells: Chemical and microbiome analysis

Erica A. Dasi[a], Jeffrey A. Cunningham[a], Emmanuel Talla[b], Sarina J. Ergas[a*]

a. Department of Civil & Environmental Engineering, University of South Florida (USF), 4202 E. Fowler Ave, ENG 030, Tampa, FL 33620, USA

b. Aix Marseille Univ, CNRS, Laboratoire de Chimie Bactérienne (LCB), F-13009, Marseille, France

*Corresponding author: sergas@usf.edu (S.J. Ergas); Address: 4202 E. Fowler Avenue, ENG 030, Tampa, FL 33620-5350, USA

Commented [A1]: One corresponding author

Abstract

This research evaluated the metal-sulfide mineral, sphalerite, as an electron donor for autotrophic denitrification, with and without oyster shells (OS). Batch reactors containing sphalerite simultaneously removed NO_3^- and PO_4^{3-} from groundwater. OS addition minimized NO_2^- accumulation and removed 100% PO_4^{3-} in approximately half the time compared with sphalerite alone. Further investigation using domestic wastewater revealed that sphalerite and OS removed NO_3^- at a rate of 0.76 ± 0.36 mg NO_3^--N/(L · d), while maintaining consistent PO_4^{3-} removal (~97%) over 140 days. Increasing the sphalerite and OS dose did not improve the denitrification rate. 16S rRNA amplicon sequencing indicated that sulfur-oxidizing species of *Chromatiales*, *Burkholderiale*s, and *Thiobacillus* played a role in N removal during sphalerite autotrophic denitrification. This study provides a comprehensive understanding of N removal during sphalerite autotrophic denitrification, which was previously unknown. Knowledge from this work could be used to develop novel technologies for addressing nutrient pollution.

Keywords: Sphalerite, Oyster shells, Autotrophic denitrification**,** Phosphorus removal**,** 5-Stage Bardenpho microbiome

1. Introduction

Pollution of ground and surface waters by the nutrients nitrogen (N) and phosphorus (P) remains a major cause of eutrophication and can increase the risk of methemoglobinemia, specific cancers, and birth defects in humans (Ward et al., 2018). Nutrient sources include poorly functioning centralized or onsite wastewater treatment facilities, fertilizers, livestock wastes, and urban and agricultural runoff. Small community water systems (CWS) have limited access to technological and financial resources for nutrient control, making them especially vulnerable to N and P pollution (Gasteyer, 2010). For example, more than 5,000 small CWS in the US violated the federal maximum contaminant level of 10 mg/L NO_3^--N in 2013 (Oxenford and Barret, 2016). Nutrient control is therefore essential to preserve water resources, especially in small community settings.

Autotrophic denitrification is a promising approach to treat NO_3^--contaminated waters (Hu et al., 2020). Autotrophic denitrifiers use inorganic electron donors, such as hydrogen gas (Ergas and Reuss, 2001) or elemental sulfur (S^0) (Sengupta et al., 2007), and inorganic carbon sources for cell synthesis. In some contexts, the use of inorganic electron donors reduces secondary contamination that can occur when organic carbon is carried over to the product water (Ergas and Aponte-Morales, 2014). Autotrophic denitrifiers also have low sludge production rates due to their slow growth yields (Sierra-Alvarez et al., 2007). This may lower backwashing and sludge disposal costs for certain denitrification designs (e.g., packed or fluidized beds; Hu et al., 2020). Thus, overall, autotrophic denitrification may offer an inexpensive and low-complexity approach to address nutrient pollution in various settings.

Metal sulfide minerals, such as pyrite (FeS_2) and pyrrhotite ($Fe_{(1-x)}S$ (x = 0 to 0.2)), are widespread and abundant in the earth's crust and have attracted interest for autotrophic denitrification (Li et al., 2013; Kong et al., 2016; Li et al., 2016; Ge et al., 2019; Hu et al., 2020).

These minerals can be used as both slow-release electron donors and biofilm carriers in packed-bed reactors (Tong et al., 2017). Pu et al. (2014) observed NO_3^- removal efficiencies exceeding 99% in batch pyrite denitrification reactors used for treating groundwater. Metal sulfide minerals can also support simultaneous NO_3^- and P removal by forming hydroxides (e.g., $Fe(OH)_3$) that promote PO_4^{3-} adsorption (Li et al., 2013; 2016). Li et al. (2013) observed NO_3^- and PO_4^{3-} removal efficiencies exceeding 99% in ferrous sulfide (FeS) batch reactors applied to treat wastewater. Furthermore, a pyrrhotite autotrophic denitrification biofilter was shown to remove 96% of both total oxidized nitrogen and PO_4^{3-} from wastewater (Li et al., 2016). The success of pyrite, ferrous sulfide, and pyrrhotite in supporting nutrient removal suggests that other previously untested metal sulfide minerals might have this capability. Sphalerite ((Zn,Fe)S) might be a promising substrate for denitrification as it primarily contains sulfide (32-33%). Its trace mental content may also support PO_4^{3-} removal (45-67% zinc, ≤ 18% iron, ≤ 28% cadmium, and ≤ 3% manganese; Anthony et al., 1990).

Oyster shells are a widespread by-product of the global shellfish industry and can be applied as a low-cost material to support N and P removal from water. They are composed of approximately 97% calcium carbonate in a scleroprotein matrix (Asaoka et al., 2009). Oyster shells enhance sulfur-driven autotrophic denitrification by serving as a slow-release alkalinity source (Sengupta et al., 2007), surface for biofilm attachment (Tong et al., 2017), and possibly an organic carbon source for mixotrophic (i.e., mixed autotrophic and heterotrophic) denitrification (Asaoka et al., 2009; Tong et al., 2017). Previous research demonstrated that a pyrite-based autotrophic denitrification biofilter containing oyster shells achieved a higher NO_3^- removal efficiency (90%) and lower SO_4^{2-} production (150 mg/L) than pyrite alone (Tong et al., 2017). Oyster shells were also shown to achieve long-term (210 d) PO_4^{3-} removal (96%) when applied as an adsorbent (Park and Polprasert, 2008).

Commented [A2]: Removed "in our laboratory" from text.

Prior studies have investigated the microbial community structure in denitrifying systems with metal sulfide minerals to understand the biological mechanisms of N removal (Pu et al., 2014; Kong et al., 2016; Li et al., 2016). *Thiobacillus* is the most reported sulfur-oxidizing and denitrifying genus in laboratory and pilot-scale studies with pyrite and pyrrhotite (Kong et al., 2016; Li et al., 2016; Ge et al., 2019). Kong et al. (2016) are, to date, the only authors that have explored the microbial community structure when sulfur (S) mineral and oyster shells are combined. The authors confirmed that mixotrophic processes occurred in a pyrite and oyster shell-based biofilter by the presence of both autotrophic and heterotrophic bacteria, such as *Thiobacillus* and *Thauera*, respectively (Kong et al., 2016).

Multiple research gaps exist regarding the use of metal sulfide minerals for autotrophic denitrification. First, no prior published studies have investigated the use of sphalerite as an electron donor for autotrophic denitrification. Second, few studies have investigated the combined effect of oyster shells and metal sulfide minerals on autotrophic denitrification. Based on a review of the prior literature, pyrite is the only metal sulfide mineral that has been studied in conjunction with oyster shells (Tong et al. 2017; 2018; Kong et al., 2016). Third, no reports have explored the contribution of the microbial community to denitrification when oyster shells and metal sulfide minerals other than pyrite are combined. Expanding knowledge in these areas can help researchers identify appropriate substrates to use in autotrophic denitrifying technologies.

The broad goal of this research is to improve the understanding of metal sulfide mineral-based denitrification to support the development of novel technologies that can address nutrient pollution globally. The specific objectives are to: (1) Examine the denitrification performance of sphalerite by quantifying NO_3^- and PO_4^{3-} removal as well as by monitoring SO_4^{2-} by-product formation; (2) Evaluate the effect of combining sphalerite and oyster shells on denitrification performance; (3) Assess the effect of sphalerite and oyster shell dose on denitrification

performance; and (4) Uncover the microbial community during sphalerite autotrophic denitrification, with and without oyster shells, to understand N-transformations as well as N removal mechanisms.

2. Materials and methods

Work was completed in three phases, each employing batch reactor studies. Phase 1 investigated the denitrification performance of sphalerite using groundwater contaminated by NO_3^- and PO_4^{3-}. Phase 2 evaluated the effect of oyster shell addition on the removal of both NO_3^- and PO_4^{3-} from groundwater. Phase 3 assessed the effect of sphalerite and oyster shell dose on nutrient removal in a larger scale reactor with nitrified domestic wastewater instead of groundwater. The microbial community was characterized in each phase to elucidate the N-transformations and N removal mechanisms linked to sphalerite autotrophic denitrification.

2.1 Materials

Sphalerite was obtained from Fisher Scientific (Waltham, Massachusetts) for use in Phases 1 and 2. Sphalerite from the Middle Tennessee Mines was used for Phase 3 (Nyrstar Corporation, Budel, Netherlands). Oyster shells were purchased from a local agricultural supplier (Shells, Tampa, Florida). S^0 pellets (4.0–6.0 mm; 90% sulfur and 10% bentonite), which were used as a positive control, were obtained from Southern Aggregates (Palmetto, Florida). Sphalerite samples were characterized using powder X-ray diffraction as described by Dasi (2022). X-ray patterns confirmed the presence of sphalerite in both sources (Dasi, 2022). Sphalerite and oyster shells were crushed manually and sieved to a particle size between 1-2 mm. The crushed minerals were pre-treated as described by Pu et al. (2014) prior to use in reactors. Briefly, the crushed minerals were soaked in a 10% (v/v) hydrochloric acid solution, rinsed with

Commented [A3]: Removed spectra of x-ray diffraction analysis from the supplemental materials.

deionized water, dried at 103 °C, and maintained under anoxic conditions until use. Oyster shells were rinsed with deionized water and dried at 20 ± 2 °C.

2.2 Inoculum and water sources

Settled mixed liquor suspended solids (MLSS) were collected from the Hillsborough County Northwest Regional Water Reclamation Facility (NWRWRF; Tampa, Florida), which applies a five-stage Bardenpho process for biological nutrient removal. For all phases, the MLSS was used as an inoculum source containing a diverse microbial community to select a unique consortium of denitrifying bacteria that oxidize sphalerite (Zhou et al., 2017). Groundwater from the University of South Florida's Botanical Gardens (0.8 ± 0.69 mg/L NO_3^--N, 0.0 ± 0.0 mg/L NH_4^+-N, 1.1 ± 1.1 mg/L PO_4^{3-}-P, 173.6 ± 33.6 mg/L alkalinity [as $CaCO_3$], and 12.5 ± 2.5 mg/L chemical oxygen demand [COD]) was used as a water source for Phases 1 and 2.The groundwater was filtered through a 0.45-µM mixed cellulose ester membrane (Fisher Scientific, Waltham, Massachusetts) before use. Secondary clarifier effluent collected from the Hillsborough County Northwest Regional Water Reclamation Facility was used as a domestic wastewater source in Phase 3. Analytical-grade KNO_3, $NaHCO_3$, NH_4Cl, K_2HPO_4, and KH_2PO_4 (Fisher Scientific, Waltham, Massachusetts) were added to the water sources to achieve initial target concentrations of approximately 40–100 mg/L NO_3^--N, 300 mg/L alkalinity as $CaCO_3$, 1–10 mg/L NH_4^+-N, and 1–10 mg/L PO_4^{3-}-P, respectively.

2.3 Batch reactor setup

Table 1 provides information on the batch studies. Phase 1 and 2 batch reactors were constructed using 250 mL glass anaerobic serum bottles with septum seal crimp caps. To investigate the effect of system scale and sphalerite mass on denitrification performance, Phase 3 batch reactors were constructed in 1 L glass bottles with screw caps drilled to fit two 5-mL plastic

pipettes. The first pipette served as a sampling port to withdraw liquid. The second pipette allowed the headspace to be connected to a FlexFoil gas sample bag (SKC, Inc., Eighty-Four, Pennsylvania) containing N_2 gas. This allowed the reactors to remain anoxic as liquid samples were removed from the bottles. In all three phases, reactors (except for uninoculated controls) were inoculated with 300 mg/L volatile suspended solids from the NWRWRF. All inoculated reactor types in the first two phases were tested in triplicate. Single batch reactors were assembled to test each uninoculated (UN) control during Phases 1 and 2 as well as the experimental and control samples of Phase 3. Following construction and inoculation, reactors were flushed with N_2 gas for 7 min to provide anoxic conditions, then incubated in a dark constant-temperature room at 22 ± 2 °C.

In Phase 1, denitrification was monitored in four types of batch reactors: (a) Experimental reactors containing sphalerite were used to assess its ability to support nutrient removal by autotrophic denitrification; (b) Positive controls containing S^0 and oyster shells (OS) were used as a basis of comparison to assess the performance of sphalerite; (c) An uninoculated (UN) reactor, containing sphalerite but without MLSS, was used as a negative control to test for abiotic removal of NO_3^- and PO_4^{3-}; and (d) Inoculum-only control reactors, which were inoculated with MLSS but did not contain sphalerite or OS, were used to test for heterotrophic denitrification supported by endogenous decay of the MLSS.

In Phase 2, denitrification was examined using an inoculum-only control and three different types of batch reactors: (a) Experimental reactors containing sphalerite and OS were combined at a 3:1 mass ratio (Table 1) to evaluate the effect of combining these substrates on nutrient removal; (b) Reactors containing OS and MLSS were used to assess if biological nutrient removal can be supported by OS alone; and (c) an UN reactor containing OS was used to test for abiotic reactions induced by the OS.

In Phase 3, denitrification was investigated over three cycles. In cycle 1, sphalerite and OS were added a 4:1 ratio (Table 1). After 30 days, additional sphalerite and OS were added to evaluate the effect on denitrification performance for two additional cycles. This phase also employed the inoculum-only control as described above. Whenever the NO_3^- concentration in the reactors fell below 6 mg/L (as N) during Phase 3, half of the liquid volume was replaced with the fresh prepared wastewater to begin another cycle.

2.4 Sampling and Analysis

Samples of supernatant were collected and filtered through 0.45-µM membrane filters (Fisher Scientific, Waltham, MA) for measurement of anions, cations, total N (TN), total P (TP), and COD. Anions and cations were measured using 881 Compact IC Pro anion or cation ion chromatography systems (Metrohm AG, Herisau, Switzerland) based on *Standard Methods* 4110B (APHA et al., 2017). TN, TP, and COD were measured using the HACH methods 827, 844, and 8000, respectively. Unfiltered liquid samples were used to measure alkalinity and pH using *Standard Methods* 2320B (APHA et al., 2017) and a calibrated Orion 5-Star meter (Thermo Scientific, Beverly, MA). Samples were collected for DNA extraction to examine the microbial community on the days listed in Table 1. MLSS samples were also collected from the NWRWRF to characterize the initial microbial community of the wastewater inoculum and to evaluate the microbial community change over time.

2.5 Microbial community analysis

16S rRNA amplicon sample preparation and sequencing were performed as described by He et al. (2021). Briefly, genomic DNA was extracted according to the manufacturer's instructions of the AllPrep PowerViral DNA/RNA Kit (QIAGEN, INC., Hilden, Germany). PCR amplification, library preparation, and sequencing were performed by Applied Biological

206 Materials, Inc. (Vancouver, Canada). The raw sequencing reads were deposited into the NCBI
207 Sequence Read Archive database under the accession numbers: PRJNA830589 and
208 PRJNA926698.
209 Processing of the raw sequencing data was performed using the Galaxy server (Afgan et
210 al., 2018) and the "16S Microbial Analysis with Mothur" protocol (Hiltemann et al., 2019) with
211 the modifications described by Dasi (2022). After clustering similar sequences into operational
212 taxonomic units (OTUs), the data were downloaded from the Galaxy server for additional
213 organizing and visualization. Note that each OTU is intended to represent a taxonomic group of
214 bacteria (e.g., *Thiobacillus*) that was identified in a sample.
215 In-house Perl scripts were used to calculate each sample's average OTU percent
216 abundance and OTU change over time. Changes in microbial community structure were
217 expressed as fold change, which was calculated as the average OTU percent abundance at the
218 final time over the abundance at the initial time. Calculated values used to visualize the microbial
219 community composition and change are available in Dasi et al. (2023). Two figure types were
220 created using RStudio® (version 1.2.5042) (R Core Team, 2020): (1) stacked bar charts showing
221 the relative microbial community composition, and (2) bar charts depicting the microbial
222 community change by a factor of two (i.e., $\log_2$ fold change). Note that some OTUs were
223 undetected (i.e., 0%) in a sample at the initial or final time points. For these, $\log_2$ fold change
224 values could not be calculated, and the OTU was described as either "appeared" or
225 "disappeared." Uncharacterized OTUs to at least the order level were combined by taxonomic
226 rank to represent phylum_unclassified and class_unclassified for both figure types. In addition,
227 the term "unclassified" was removed from OTUs only classified to the order and family ranks.
228 Unknown OTUs are characterized as bacteria_unclassified in the figures and Dasi et al. (2023).
229

2.6 Data analysis

Average denitrification rates were estimated by Equation 1, using the final and initial NO_3^--N concentrations.

$$\text{Average denitrification rate } \left(\frac{\text{mg}}{\text{L}\cdot\text{d}}\right) = \frac{C_i - C_f}{t_f - t_i} \quad (1)$$

where C and t denote the NO_3^- concentration (mg N/L) and time (d), respectively.

Total organic nitrogen (TON) concentration was calculated by subtracting the total inorganic nitrogen (TIN = NO_3^--N + NO_2^--N + NH_4^+-N) from the TN concentration. Total organic phosphorus (TOP) concentration was estimated calculated by subtracting the PO_4^{3-}-P concentration from the TP concentration.

Theoretical S/N ratios (i.e., SO_4^{2-}produced/NO_3^--N consumed) were estimated for S^0 (Equation 2, Batchelor and Lawrence, 1978) and sphalerite (Equations 3 and 4) autotrophic denitrification. Equations 3 and 4 were developed for the two different sphalerite sources using the method of McCarty (1975), thermodynamic data from Lide (1991) and Tagirov and Seward (2010), and assuming empirical formulas for sphalerite, based on the X-ray diffraction patterns (Dasi, 2022).

$$1.10\ S^0 + 0.40\ CO_2 + NO_3^- + 0.76\ H_2O + 0.08\ NH_4^+ \Rightarrow$$
$$0.08\ C_5H_7O_2N + 0.50\ N_2 + 1.10\ SO_4^{2-} + 1.28\ H^+ \quad (2)$$

$$0.746\ Zn_{0.628}Fe_{0.372}S + 0.250\ CO_2 + NO_3^- + 1.19\ H_2O + 0.0625\ NH_4^+ + 0.0625\ HCO_3^- \Rightarrow$$
$$0.468\ Zn(OH)_2 + 0.278\ Fe(OH)_3 + 0.0625\ C_5H_7O_2N + 0.50\ N_2 + 0.746\ SO_4^{2-} + 0.493\ H^+ \quad (3)$$

$$0.764\ Zn_{0.825}Fe_{0.175}S + 0.250\ CO_2 + NO_3^- + 1.159\ H_2O + 0.0625\ NH_4^+ + 0.0625\ HCO_3^- \Rightarrow$$
$$0.631\ Zn(OH)_2 + 0.134\ Fe(OH)_3 + 0.0625\ C_5H_7O_2N + 0.50\ N_2 + 0.764\ SO_4^{2-} + 0.529\ H^+ \quad (4)$$

Statistical testing was performed using the Origin 9 software (OriginLab, 2021). Replicates were examined to determine whether a sample was well-modeled by a normal distribution using the Anderson-Darling test (Anderson and Darling, 1952). Those samples with replicates that followed a normal distribution were tested using parametric statistics. One-way ANOVA testing was applied to compare three or more independent samples. Alternatively, two sample t-testing was used to compare fewer than three independent samples. Results from the one-way ANOVA testing were only considered for samples that had equal variance with the Brown-Forsythe test (Brown and Forsythe, 1974). The Welch t-statistic was considered during two sample t-testing for comparisons with unequal variance (Welch, 1947). Comparisons with *p* values less than 0.05 were considered significantly different.

3. Results and discussion

3.1 Denitrification performance of sphalerite, with and without oyster shells

3.1.1 N removal

Figure 1 shows the N species concentration profiles for Phases 1 and 2. NO_3^- reduction in the controls was generally as anticipated. NO_3^- was undetected in the S^0 + OS positive control by day 13 (Fig. 1A), demonstrating that the methodology applied was sufficient to support autotrophic denitrification. As a result, analysis of the denitrification performance beyond day 13 for the S^0 + OS batch reactors was discontinued. The NO_3^- concentration profile in the UN reactors was relatively stable, indicating that neither sphalerite nor OS directly reduced NO_3^- without a specialized microbial community (see supplementary materials). NO_3^- removal in the inoculum-only control was higher than expected (Fig. 1A and 1B), indicating that particulate organic matter in the inoculum or endogenous decay of the inoculum provided substrate for heterotrophic denitrification in the biotic reactors.

Gradual NO_3^- removal was observed in the batch reactors with sphalerite (Fig. 1A and 1B). Initially, NO_3^- concentrations in the sphalerite and inoculum-only reactors tracked closely, suggesting the heterotrophic denitrification might have been the main NO_3^- removal mechanism at early times. However, mean NO_3^- concentrations of the sphalerite reactors remained significantly different than the inoculum-only control after days 34 and 13 of Phase 1 and Phase 2, respectively ($p < 0.030$; see supplementary materials). These results indicate that although heterotrophic denitrification initially drove NO_3^- reduction in the batch reactors with sphalerite, mineral addition eventually increased NO_3^- removal. NO_3^- removal was also accompanied by NH_4^+ release during both phases (Fig. 1E and 1F), which might be due to dissimilatory nitrate reduction to ammonium (DNRA). This is discussed in more detail below.

Average denitrification rates and S/N ratios for Phases 1 and 2 can be found in the supplementary materials. Although the NO_3^- removal rate for the batch reactors with sphalerite was slower than the S^0 + OS control (Fig. 1A and 1B), the average denitrification rates for the reactors with sphalerite (1.0 mg/L*d) and sphalerite + OS (1.14 mg/L*d) were close to those observed by Li et al. (2022), who performed similar batch studies with pyrite (~ 1.1 mg/L*d). The use of solid-phase electron donors, such as sphalerite and pyrite, with suspended biomass in batch reactors may contribute to slow average denitrification rates. Application of these minerals in biofilm systems (e.g., packed-bed reactors) may improve their utilization by autotrophic denitrifying bacteria.

Mineral and OS addition improved N removal compared to using sphalerite as a substrate. As discussed previously, a slightly higher average denitrification rate was observed for the sphalerite + OS reactors than those with only sphalerite. TIN removal was also higher in the sphalerite + OS reactors over 67 days than those with mineral (70% vs. 60%; Fig. 1), suggesting that more NO_3^- was reduced to gaseous products. This likely occurred because NO_2^-

accumulation was lower in the sphalerite + OS batch reactors (Fig. 1C and 1D). NO_2^- accumulation possibly occurred since the NO_3^- reductase enzyme (Nar) preferentially accepts electrons over the enzyme responsible for NO_2^- reduction (i.e., Nir). As a result, NO_3^- reduction is prioritized and NO_2^- reduction delayed during denitrification (Richardson et al., 2009; Ucar et al., 2021). The high initial NO_3^- concentration of the prepared groundwater may have also inhibited the activity of the Nir enzyme, causing NO_2^- to accumulate (Fig. 1A and 1B; Glass and Silverstein, 1998). Colonization of a unique consortium of bacteria on the sphalerite + OS reactor media may have supported better N removal than the sphalerite reactors. Key microbial drivers involved in transforming N are discussed further in Section 3.3.3.

3.1.2 SO_4^{2-} By-product Formation

Figure 2 shows additional chemical results for Phases 1 and 2. Day 0 SO_4^{2-} concentrations for the reactors with sphalerite were similar to the inoculum-only control (Fig. 2A and 2B). This suggested that mineral preparation did not cause substantial surface sulfide oxidation, which could increase aqueous SO_4^{2-} concentration in the reactors. As expected, SO_4^{2-} production was only observed in the reactors containing either S^0 or sphalerite (Fig. 2A and 2B). SO_4^{2-} in the S^0 + OS positive control was below the maximum theoretical concentration (~860 mg/L) based on Equation (2), but sufficiently high to confirm that autotrophic denitrification occurred (Fig. 2A). In contrast, much lower and gradual SO_4^{2-} production was observed in the batch reactors with sphalerite (Fig. 2A and 2B). Sphalerite oxidation is described to occur in a two-step process. During the first step, sulfide is incompletely oxidized to S^0 to form a layer on the mineral surface. Bacterial oxidation of this layer can proceed afterward, leading to the production of SO_4^{2-} (Fowler and Crundwell, 1999; Zapata et al., 2007). Heterotrophic denitrification and incomplete sulfide oxidation may have occurred simultaneously as S autotrophic bacteria were cultivated in the batch reactors with sphalerite. This might explain why the observed S/N ratios for sphalerite-

driven denitrification in Phase 1 (1.50 mg SO_4^{2-}/mg NO_3^-) and Phase 2 (1.58 mg SO_4^{2-}/mg NO_3^-) were below the theoretical value (5.1 mg SO_4^{2-}/mg NO_3^-) obtained from Equation (3). The peroxide method applied by Pu et al. (2014) could be used in future research to quantify incomplete S oxidation when sphalerite is used for autotrophic or mixotrophic denitrification.

3.1.3 P Removal

Clear P removal occurred in the batch reactors containing sphalerite (Fig. 2C and 2D). PO_4^{3-} removal was also observed in the sphalerite UN batch reactor (see supplementary materials), suggesting that abiotic processes (i.e., precipitation and adsorption) may play a role. Yang et al. (2017) found that precipitates, such as $FePO_4$ and $Fe(OH)_3$, were likely responsible for P adsorption onto pyrrhotite in anoxic packed-bed reactors. Mineral surface chemistry was not evaluated in Phases 1-3. However, sphalerite autotrophic denitrification may drive P removal mechanisms that are similar to those described by Yang et al. (2017) and involve iron and zinc (Almasri et al., 2021). PO_4^{3-} was completely removed from the sphalerite + OS reactors in approximately half the time observed for its mineral-only counterpart (Fig. 2C and 2D). OS addition most likely supported additional precipitation processes, as it contains approximately 97% calcium carbonate (Asaoka et al., 2009). Calcium released from the OS possibly precipitated with PO_4^{3-} to form hydroxyapatite ($Ca_{10}(PO_4)_6OH_2$), which could have been adsorbed onto sphalerite's surface (Khan et al., 2020).

3.2 Effect of sphalerite and oyster shells dose on denitrification performance

Phase 3 further confirms that sphalerite can be used as an electron donor for autotrophic denitrification. Figures 3 and 4 show the results obtained for this phase. Simultaneous NO_3^- removal and SO_4^{2-} production were observed during each cycle, confirming that S oxidation occurred concurrently with denitrification in the sphalerite + OS reactor (Fig. 3A and 3B). Close

Commented [A4]: Removed "our" from text.

347 tracking of the sphalerite + OS reactor's observed SO_4^- concentration profile with the theoretical
348 trend provides additional evidence of S autotrophic denitrification (Fig. 3B).
349 Mixotrophic denitrification during cycle 1 may explain the observed trends in the
350 sphalerite + OS batch reactor. Slight NO_3^- reduction and NO_2^- production were observed in the
351 inoculum-only control during cycle 1, suggesting that heterotrophic denitrification initially
352 occurred in the sphalerite + OS reactors (Fig. 3A and 3C). COD, TON, and TOP were also
353 removed from the sphalerite + OS reactor during cycle 1, which provides additional evidence of
354 heterotrophic denitrification (Fig. 4A - 4C). Based on the COD consumed and the stoichiometric
355 requirements for heterotrophic denitrification (2.86 mg COD/mg NO_3^--N; Ergas and Aponte-
356 Morales, 2014), only 4.2 mg/L NO_3^--N could have been removed by this mechanism (~ 40 mg/L
357 NO_3^--N were removed in cycle 1; Fig. 3A). Concurrent heterotrophic and autotrophic
358 denitrification during cycle 1 in the sphalerite + OS reactor may explain the observed alkalinity
359 production (Fig. 4D) and higher average denitrification rates compared to the subsequent cycles
360 (Fig. 3A). Similar SO_4^- concentration profiles between the observed and theoretical trends for the
361 sphalerite + OS reactors suggest that that heterotrophic denitrification became negligible over
362 time (Fig. 3B).
363 Results from cycles 2 and 3 suggest that increasing sphalerite and OS dose may not
364 improve NO_3^- removal. Average denitrification rates between cycles 2 and 3 declined in the
365 sphalerite + OS batch reactor (Fig. 3A). Prior research suggests that layers formed on sphalerite's
366 surface can block the diffusion of soluble substrates to autotrophic bacteria, limiting the
367 denitrification rate (Fowler and Crundwell, 1999). PO_4^{3-} removal efficiency was maintained at
368 approximately 97% during cycles 1-3 (Fig. 3E), which suggests that precipitates responsible for P
369 removal accumulated on the mineral surface. These precipitates may have limited access of
370 sulfide to denitrifying bacteria, causing the average denitrification rate to decrease each cycle.

3.2 N-transformations and removal mechanisms of sphalerite autotrophic denitrification

3.3.1 Assessment of the microbial community analysis

Information of the 16S rRNA gene libraries obtained from the Illumina-based sequencing can be found in the supplementary material. Moderate percentages of effective sequences were recovered after quality filtering of the samples. Despite this, high Good's coverage values suggest that the microbial composition for each sample is well represented by the constructed sequence libraries and thus reflects the real bacterial profile. Examination of the 16S rRNA sequence libraries indicates that the data is of sufficient quality to investigate the microbial community composition and change.

3.3.2 Microbial community of the inoculum from a full-scale five-stage Bardenpho process

The inoculum contained a diverse consortium of bacteria, which possibly supports the removal of N, P, and organics at the NWRWRF. The supplementary material shows the microbial community composition of the initial inoculum. Dominant bacteria are considered as those representing more than 0.99% of the total population. Dominant bacteria in the inoculum included *Actinomycetales* (7.0%), *Intrasporangiaceae* (6.6%), *Planctomycetaceae* (3.8%), *Aquihabitans* (2.1%), *Conexibacter* (1.8%), and *Nitrospira* (1.7%) (see supplementary materials). Phosphate accumulating organisms (PAOs) belonging to *Intrasporangiaceae* may drive enhanced biological P removal at the NWRWRF (Lee and Park, 2008), while members of *Nitrospira* likely carry out nitrification (Dueholm et al., 2022). *Aquihabitans*, *Conexibacter*, *Actinomycetales,* and *Planctomycetaceae* might also contribute to the removal of organics through the conversion of NO_3^- to NO_2^- (Dueholm et al., 2022). Taxonomic groups with species that perform complete denitrification, such as *Defluviimonas* (0.34%) and *Paracoccus* (0.11%), were also detected in

393 the inoculum (Dasi et al., 2023; Dueholm et al., 2022). It is possible that bacteria belonging to
394 these genera convert NO_3^- or N intermediates of denitrification to N_2(g) at the facility.

395 *3.3.3 Contribution of the microbial community to transforming N*

396 A synergy was observed between the microbial community and the chemistry of the
397 reactors. Figure 5 quantifies the microbial community change, considering the inoculum and
398 reactors of Phases 1 and 2. Table 2 also presents notable taxonomic groups identified during
399 these phases. Log_2 fold change values of *Intrasporangiaceae* ranged from -1.673 to -6.645 during
400 both phases, indicating that this taxonomic group decreased between 3 and 100-fold (i.e., 3 and
401 100 times) for each sample (Fig. 5A and 5B). Low bioavailable organic carbon in the reactors
402 may have resulted in volatile fatty acids concentrations below the requirements to sustain PAOs
403 of *Intrasporangiaceae*. This hypothesis is supported by the decline of *Trichococcus* (log_2 fold
404 change < -1.442; Fig. 5A and 5B), which include species that produce propionic acid by
405 fermentation (Dueholm et al., 2022). Conversely, *Ignavibacterium* emerged as a notable genus,
406 increasing in all samples at least four-fold (log_2 fold change > 2.135; Fig. 5A and 5B). Only one
407 species to date has been identified for *Ignavibacterium*, which contains a NrfAH complex that
408 converts NO_2^- to NH_4^+ during dissimilatory nitrate reduction to ammonium (DNRA) (Liu et al.,
409 2012). The presence of this genus suggests that DNRA may have caused NH_4^+ to accumulate
410 during Phases 1 and 2 (Fig. 1E and 1F). The sphalerite reactors had the greatest abundance of
411 *Ignavibacterium* compared to the others in Phase 1 (Table 2), suggesting that sulfide from the
412 mineral may have increased DNRA (Brunet and Garcia-Gill, 1996).

413 Several other taxonomic groups emerged over time to represent noteworthy populations.
414 *Chromatiaceae* and *Chromatiales* grew during both phases, with the greatest change generally
415 occurring in the reactors with sphalerite (log_2 fold change = 0.043-4.310; Dasi et al. (2023) and

Fig. 5). *Thiobacillus* also appeared and generally increased over time in the reactors containing sphalerite (Table 2). S oxidizing bacteria belonging to *Chromatiaceae*, *Chromatiales*, and *Thiobacillus* might have performed denitrification in Phases 1 and 2 (Dueholm et al., 2022). These genera had a lower abundance in the inoculum-only control compared to the sphalerite reactors by day 74 (Table 2), suggesting that less N may have been removed by autotrophic denitrification. *Candidatus Brocadiaceae* and *Candidatus Kuenenia*, whose species perform anammox (Dueholm et al., 2022), also appeared during Phase 2 after 67 days in the reactors containing OS reactors (Table 2). The presence of *Candidatus Brocadiaceae* and *Candidatus Kuenenia* in the OS-only reactors suggests that OS might have cultivated these organisms. Combined sphalerite and OS addition supported the growth of anammox, S autotrophic denitrifying, and DNRA bacteria, which likely coordinated to drive NO_3^- removal (Fig. 1B) while maintaining a low NO_2^- concentration profile (Fig. 1D). Bacterial competition in the sphalerite + OS reactors may explain the lower abundance of autotrophic denitrifying bacteria and DNRA bacteria than those with mineral (Table 2).

3.3.4 Mechanisms of N removal during sphalerite autotrophic denitrification

Figure 6 shows the microbial community structure that formed in reactor with sphalerite, OS, and domestic wastewater on day 140. Interestingly, many of the bacteria representing more than 2% of the population belong to the phylum *Proteobacteria*. This taxonomic group is metabolically diverse, containing phototrophic, chemoheterotrophic, and chemoautotrophic bacteria (Dueholm et al., 2022). Notable taxonomic groups of *Proteobacteria* included *Chromatiales* (2.4%) and *Burkholderiales* (1.1%) (Fig. 6). Like *Chromatiales*, some species of *Burkholderiales* couple S oxidation with NO_3^- reduction or complete denitrification (Dueholm et al., 2022). The presence of these orders may suggest their involvement in removing N in the

sphalerite + OS batch reactor of Phase 3. Research indicates that the microbial community structure during S autotrophic denitrification is dependent on the electron donor provided (Zhou et al., 2017). The identification of *Chromatiales* in Phases 1-3 may suggest that S autotrophic bacteria belonging to this order are possibly linked to driving sphalerite autotrophic denitrification (Table 2).

3.4 Implications and potential limitations

Based on the results, sphalerite autotrophic denitrification could be considered for future water management strategies to address nutrient pollution. The cost of sphalerite is comparable to pyrite (~ $2.30/kg; IGF, 2023). However, slower denitrification rates were observed compared with other metal sulfide minerals (Dasi, 2022) and secondary pollution of trace metals (e.g., zinc) released following S oxidation may limit the application of sphalerite autotrophic denitrification. Designs that can maintain long hydraulic residence times, such as horizontal subsurface flow constructed wetlands, might be suitable to harness sphalerite autotrophic denitrification for nutrient control, as has been done previously with pyrite (Ge et al., 2019). Future research should explore strategies to improve denitrification rates and clarify trace metal effluent quality during sphalerite autotrophic denitrification. Other areas worth exploring involve uncovering specific mechanisms of PO_4^{3-} removal and quantifying potential greenhouse gas emissions by measuring nitrous oxide production during sphalerite-driven denitrification.

4. Conclusions

This is the first study to evaluate sphalerite as an electron donor for autotrophic denitrification. Sphalerite promoted NO_3^- and PO_4^{3-} removal from groundwater. Mineral and OS addition minimized NO_2^- accumulation and promoted faster PO_4^{3-} removal than sphalerite alone. Increasing sphalerite and OS dose did not improve domestic wastewater denitrification; however,

long-term NO_3^- and PO_4^{3-} removal (140 d) was supported. 16S rRNA amplicon sequencing suggests that S oxidizing species of *Chromatiales*, *Burkholderiale*s, and *Thiobacillus* drive N removal during sphalerite autotrophic denitrification. These results provide an improved understanding of S autotrophic denitrification, which can be refined to develop solutions for nutrient control.

5. Appendix A: Supplementary materials

E-supplementary data for this work can be found in the online version of the paper.

Commented [A5]: Moved section to after conclusion section

6. Acknowledgements

This research work was supported by the USEPA (Grant No. RD 83560201-0), National Science Foundation (Grant Nos. 1243510 and 1735320), Alfred P. Sloan Foundation (Grant No. 2017-9717), Chateaubriand Fellowship Program, Florida Education Fund, and USF's Institute for Microbiomes. The LCB laboratory was funded by CNRS and Aix Marseille University.

References

Commented [A6]: References doubled spaced.

1. Afgan, E., Baker, D., Batut, B., van den Beek, M., Bouvier, D., Čech, M., Chilton, J., Clements, D., Coraor, N., Grüning, B., Guerler, A., Hillman-Jackson, J., Jalili, V., Rasche, H., Soranzo, N., Goecks, J., Taylor, J., Nekrutenko, A., Blankenberg., D., 2018. The Galaxy platform for accessible, reproducible and collaborative biomedical analyses: 2018 update. Nucleic Acids Res., 46(W1), W537-W544.
2. Almasri, D.A., Essehli, R., Tong, Y., Lawler, J., 2021. Layered zinc hydroxide as an adsorbent for phosphate removal and recovery from wastewater. RSC Adv., 11, 30172-30182.
3. Anderson, T.W., Darling, D.A., 1952. Asymptotic Theory of Certain "Goodness of Fit" Criteria Based on Stochastic Processes. Ann. Math. Statist. 23(2), 193-212.

4. Anthony, J.W., Bideaux, R.A., Bladh, K.W., Nichols, M.C., 1990. Handbook of Minerology. Mineralogical Society of America, Chantilly, VA, USA.
5. APHA, AWWA, WEF, 2017. Standard Methods for the Examination of Water & Wastewater. 23rd Edition. American Public Health Association, American Water Works Association, and Water Environment Federation. Washington, D.C., USA
6. Asaoka, S., Yamamoto, T., Kondo, S., Shinjiro, H., 2009. Removal of hydrogen sulfide using crushed oyster shell from pore water to remediate organically enriched coastal marine sediments. Bioresour. Technol., 100(18), 4127-4132.
7. Batchelor, B., Lawrence, A.W., 1978. Autotrophic denitrification using elemental sulfur. J. Water Pollut. Control Fed., 50(8), 1986-2001.
8. Brown, M.B., Forsythe, A.B., 1974. Robust Tests for the Equality of Variances, J. Am. Stat. Assoc. 69(346), 364-367.
9. Brunet, R.C., Garcia-Gil, L.J., 1996. Sulfide-induced dissimilatory nitrate reduction to ammonia in anaerobic freshwater sediments. Fems Microbiol. Ecol. 21(2), 131-138.
10. Dasi, E.A., 2022. Elemental Sulfur and Metal Sulfide Minerals for Autotrophic Denitrification: Applications to Aquaculture, Groundwater Treatment, and Domestic Wastewater Treatment. USF Tampa Graduate Theses and Dissertations.
11. Dasi, E.A., Cunningham, J.A., Talla, E., Ergas, S.J., 2023. Microbial community dataset for sphalerite and oyster shell denitrification study, Mendeley Data, V2, doi: 10.17632/h696jj4pf8.1
12. Dueholm, M. K. D., Nierychlo, M., Andersen, K.S., Rudkjøbing, V., Knutsson, S., Albertsen, M., Nielsen, P.H., 2022. MiDAS 4: A global catalogue of full-length 16S rRNA gene sequences and taxonomy for studies of bacterial communities in wastewater treatment plants. Nat. Commun. 13(1908), 1-15.

13. Ergas, S.J., Reuss, A. (2001) Hydrogenotrophic denitrification of drinking water using a hollow fiber membrane bioreactor, J. Water Supply Res. T., 50(3):161-171.
14. Ergas, S.J, Aponte-Morales, V., 2014. Biological Nurtient Removal. In: Ahuja, S. (Ed.) Comprehensive Water Quality and Purification. Elsevier Inc. Amsterdam, Netherlands.
15. Fowler, T.A., Crundwell, F.K., 1999. Leaching of zinc sulfide by Thiobacillus ferroxidans: Bacterial oxidation of the sulfur product layer increases the rate of zinc sulfide dissolution at high concentrations of ferrous iron. Appl. Environ. Microbiol., 65(12), 5285-5292.
16. Gasteyer, S., 2010. Are small community water systems more at risk than other systems? https://www.yumpu.com/en/document/read/24194396/are-small-community-water-systems-more-at-risk-than-other-
17. Ge, Z., Wei, D., Zhang, J., Hu, J., Liu, Z., Li, R., 2019. Natural pyrite to enhance simultaneous long-term nitrogen and phosphorus removal in constructed wetland: three years of pilot study. Water Res., 148, 153-161.
18. He, Q., Dasi, E. A., Cheng, Z., Talla, E., Main, K., Feng, C., Ergas, S.J., 2021. Wood and sulfur-based cyclic denitrification filters for treatment of saline wastewaters. Bioresour. Technol. 328, 124848-124857.
19. Hiltemann, S., Batut, B., Clements, D., 2019. 16S Microbial Analysis with mothur (extended) (Galaxy Training Materials). /training-material/topics/metagenomics/tutorials/mothur-miseq-sop/tutorial.html Online
20. Hu, Y., Wu, G., Li, R., Xiao, L., Zhan, X., 2020. Iron sulphides mediated autotrophic denitrification: an emerging bioprocess for nitrate pollution mitigation and sustainable wastewater treatment. Water Res., 179, 115914-115939.
21. Intergovernmental Forum on Mining, Minerals, Metals and Sustainable Development (IGF), 2023. Mineral pricing. https://www.igfmining.org/beps/current-topics/mineral-pricing/

22. Khan, M.D., Chottitisupawong, T., Hong, Vu, H.H.T., Ahn, J.W., Kim, G.M., 2020. Removal of phosphorus from an aqueous solution by nanocalcium hydroxide derived from waste bivalve seashells: mechanism and kinetics. ACS Omega., 5, 21, 12290-12301.
23. Kong, Z., Li, L., Feng, C., Dong, S., Chen, N., 2016. Comparative investigation on integrated vertical-flow biofilters applying sulfur-based and pyrite-based autotrophic denitrification for domestic wastewater treatment. Bioresour. Technol., 211, 125-135.
24. Lee, H.W. and Park, Y.K., 2008. Characterizations of denitrifying polyphosphate-accumulating bacterium *Paracoccus* sp. strain YKP-9. J. Microbiol. Biotechnol., 18(12), 1958-1965
25. Li, R.H., Niu, J.M., Zhan, X.M., 2013. Simultaneous removal of nitrogen and phosphorus from wastewater by means of FeS-based autotrophic denitrification. Water Sci. Technol., 67(12), 2761-2767.
26. Li, R., Morrison, L., Collins, G., Li, A., Zhan, X., 2016. Simultaneous nitrate and phosphate removal from wastewater lacking organic matter through microbial oxidation of pyrrhotite coupled to nitrate reduction. Water Res., 96, 32-41.
27. Li, R., Zhang, Y., Guan, M., 2022. Investigation into pyrite autotrophic denitrification with different mineral properties. Water Res., 221, 118763-118771.
28. Lide, D.R., 1991. CRC Handbook of Chemistry and Physics. 71st edition. CRC Press, Boca Raton, FL, USA
29. Liu, Z., Frigaard, N. U., Vogl, K., Iino, T., Ohkuma, M., Overmann, J., Bryant, D. A., 2012. Complete Genome of Ignavibacterium album, a Metabolically Versatile, Flagellated, Facultative Anaerobe from the Phylum Chlorobi. Front. Microbiol., 3, 1-15.
30. McCarty, P.L., (1975) Stoichiometry of biological reactions. Prog. Water Technol. 7, 157-172.

31. OriginLab Corporation, 2021. OriginPro®, Northampton, MA, USA.
32. Oxenford, J. L., Barrett, J. M., 2016. Understanding small water system violations and deficiencies. J. Am. Water Works Assoc., 108(3), 31-37.
33. Park, W.H, Polprasert, C., 2008. Phosphorus adsorption characteristics of oyster shells and alum sludge and their application for nutrient control in constructed wetland system. J. Environ. Sci. Health A Tox. Hazard Subst. Environ. Eng., 43(5), 511–517.
34. Pu, J., Feng, C., Liu, Y., Kong, Z., Chen, N., Tong, S., Hao, C., Liu, Y., 2014. Pyrite-based autotrophic denitrification for remediation of nitrate contaminated groundwater. Bioresour. Technol., 173, 117-123.
35. R Core Team (2020). R: A language and environment for statistical computing. R Foundation for Statistical Computing, Vienna, Austria. URL https://www.R-project.org/.
36. Richardson, D., Felgate, H., Watmough, N., Thomson, A., Baggs, E., 2009. Mitigating release of the potent greenhouse gas N_2O from the nitrogen cycle - could enzymatic regulation hold the key? Trends Biotechnol., 27(7), 388-397.
37. Sengupta, S., Ergas, S.J., Lopez-Luna, E., 2007. Investigation of solid-phase buffers for sulfur-oxidizing autotrophic denitrification. Water Environ Res., 79(13), 2519-2526.
38. Shih, J.S., Harrington, W., Pizer, W.A., Gillingham, K., 2006. Economies of scale in community water systems. J. Am. Water Works Ass., 98(9), 100-108.
39. Sierra-Alvarez, R., Beristain-Cardoso, R., Salazar, M., Gomez, J., Razo-Flores, E., Field, J.A., 2007. Chemolithotrophic denitrification with elemental sulfur for groundwater treatment. Water Res., 41(6), 1253-1262.
40. Tagirov, B.R., Seward, T.M., 2010. Hydrosulfide/sulfide complexes of zinc to 250 °C and the thermodynamic properties of sphalerite. Chem. Geol., 269(3-4), 301-311.

41. Tong S., Stocks, J.L., Rodriguez-Gonzalez, L.C., Feng, C., Ergas, S.J., 2017. Effect of oyster shell medium and organic substrate on the performance of a particulate pyrite autotrophic denitrification (PPAD) process. Bioresour. Technol., 244, 296-303.
42. Tong, S., Rodriguez-Gonzalez, L.C., Payne, K.A., Stocks, J.L., Feng, C., Ergas, S.J., 2018. Effect of pyrite Pretreatment, particle size, Dose, and biomass concentration on particulate pyrite autotrophic denitrification of nitrified domestic wastewater. Environ. Eng. Sci., 35(8), 875-886.
43. Ucar, D., Di Capua, F., Yücel, A., Nacar, T., Sahinkaya, E., 2001. Effect of nitrogen loading on denitrification and filtration performances of membrane bioreactors fed biogenic and chemical elemental sulfur. J. Chem. Eng., 419, 129514-129524.
44. Ward, M.H., Jones, R.R., Brender, J.D., de Kok, T.M., Weyer, P.J., Nolan, B.T., Villanueva, C.M., van Breda, S.G., (2018). Drinking water nitrate and human health: an updated review. Int. J. Environ. Res. Publ. Health, 15, 1557-1588.
45. Welch, B.L., 1947. The generalisation of students' problem when several different population variances are involved. Biometrika. 34(1-2):28-35.
46. Yang, Y., Chen, T., Morrison, L., Gerrity, S., Collins, G., Porca, E., Li, R., Zhan, X., 2017. Nanostructured pyrrhotite supports autotrophic denitrification for simultaneous nitrogen and phosphorus removal from secondary effluents. Chem. Eng. J., 328(15), 511-518.
47. Zapata, D.M., Márquez, M.A., Ossa, D.M., 2007. Sulfur product layer in sphalerite biooxidation: Evidence for a mechanism of formation. Adv. Mat. Res., 20-21, 134-138.
48. Zhou, W., Li, Y., Liu, X., He, S., Huang, J.C., 2017. Comparison of microbial communities in different sulfur-based autotrophic denitrification reactors. Appl. Microbiol. Biotechnol. 101, 447-453.

Figure Captions

Fig. 1. Phase 1 and 2 batch reactor N concentration profiles. (A, C, E) Phase 1. (B, D, F) Phase 2.

Fig. 2. Phase 1 and 2 batch reactor SO42- and PO43- concentration profiles. (A, C) Phase 1. (B, D) Phase 2.

Fig. 3. Phase 3 batch reactor chemical profiles. (A) Nitrate. (B) Sulfate. (C) Nitrite. (D) Ammonium. (E) Phosphate. The vertical lines indicate the beginning of another cycle, after half the reactors' liquid volume was replaced with fresh domestic wastewater. ADR = Average denitrification rate of the sphalerite + OS batch reactor expressed in mg/(L·d).

Fig. 4. Additional chemical measurements of the Sphalerite + OS batch reactor during Phase 3, cycle 1. (A) N profile. (B) P profile. (C) Chemical oxygen demand. (D) Alkalinity. (E) pH.

Fig. 5. Relative change in the microbial community composition between the batch reactors and initial inoculum. (A) Phase 1. (B) Phase 2. Bacteria representing ≥ 0.1% of the total reads and that have Log2 fold changes between -5.0 and 3.2 in at least one of the samples are shown.

Fig. 6. Relative abundance of bacteria in the Sphalerite + OS batch reactors of Phase 3. Most bacteria that are shown are ≥ 2% in abundance. Others is comprised of bacteria that are less than 2% of the total population. Bacteria with an asterisk mark are members of the phylum *Proteobacteria*.

635 Fig. 1
636

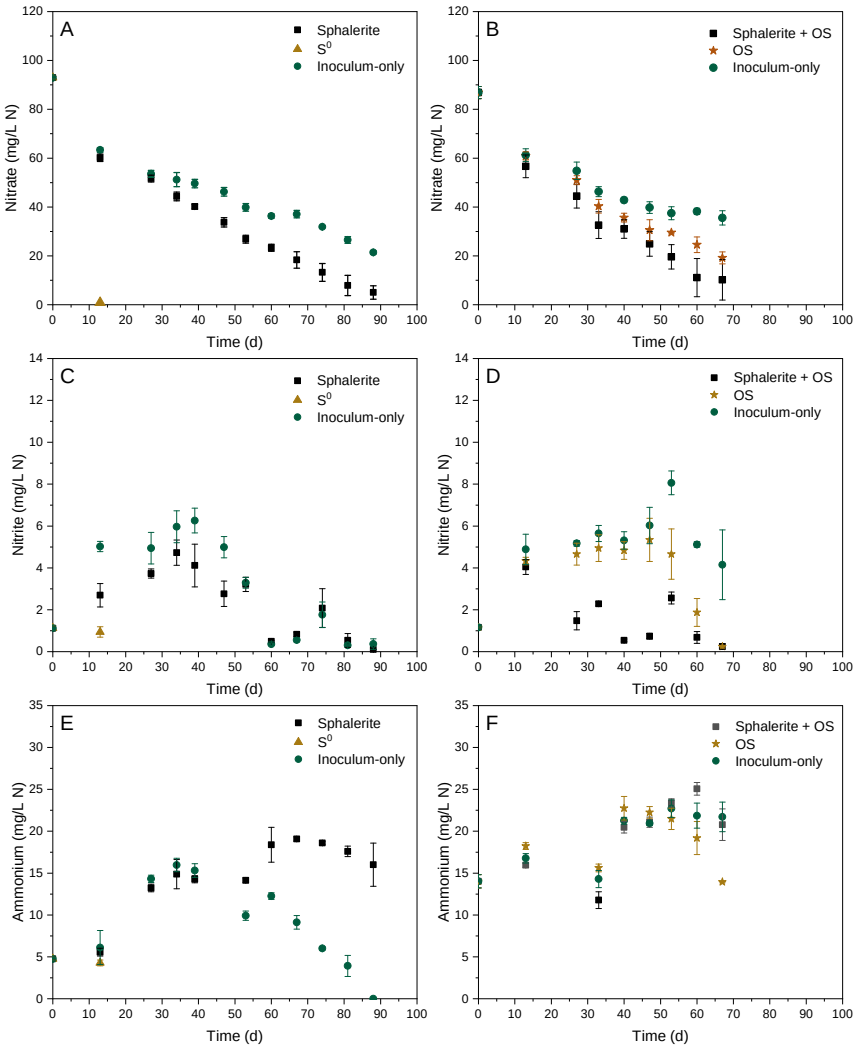

637
638
639
640

Fig. 2

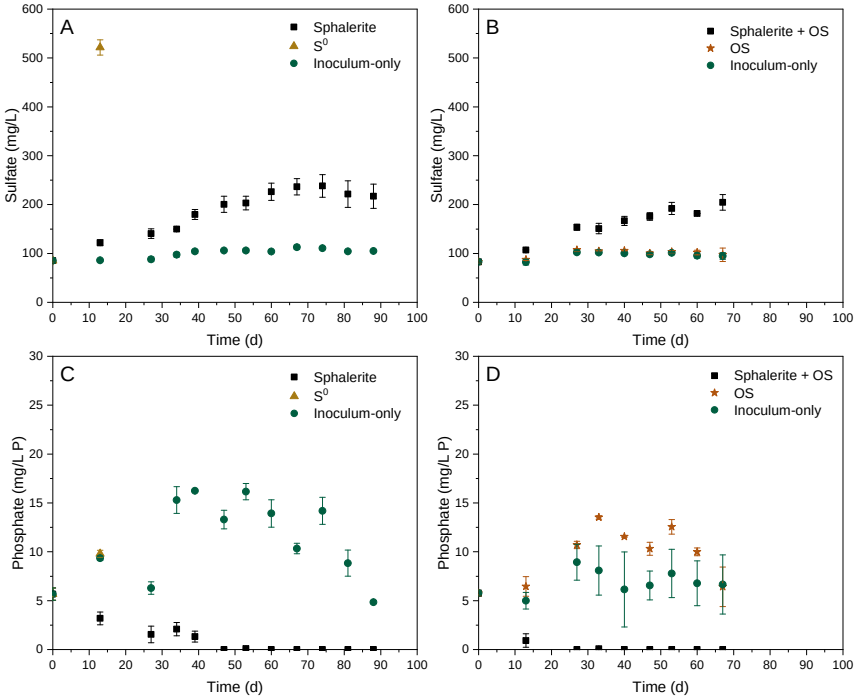
A
Sphalerite
S0
Inoculum-only
Sulfate (mg/L)
Time (d)
B
Sphalerite + OS
OS
Inoculum-only
Sulfate (mg/L)
Time (d)
C
Sphalerite
S0
Inoculum-only
Phosphate (mg/L P)
Time (d)
D
Sphalerite + OS
OS
Inoculum-only
Phosphate (mg/L P)
Time (d)

661 Fig. 3

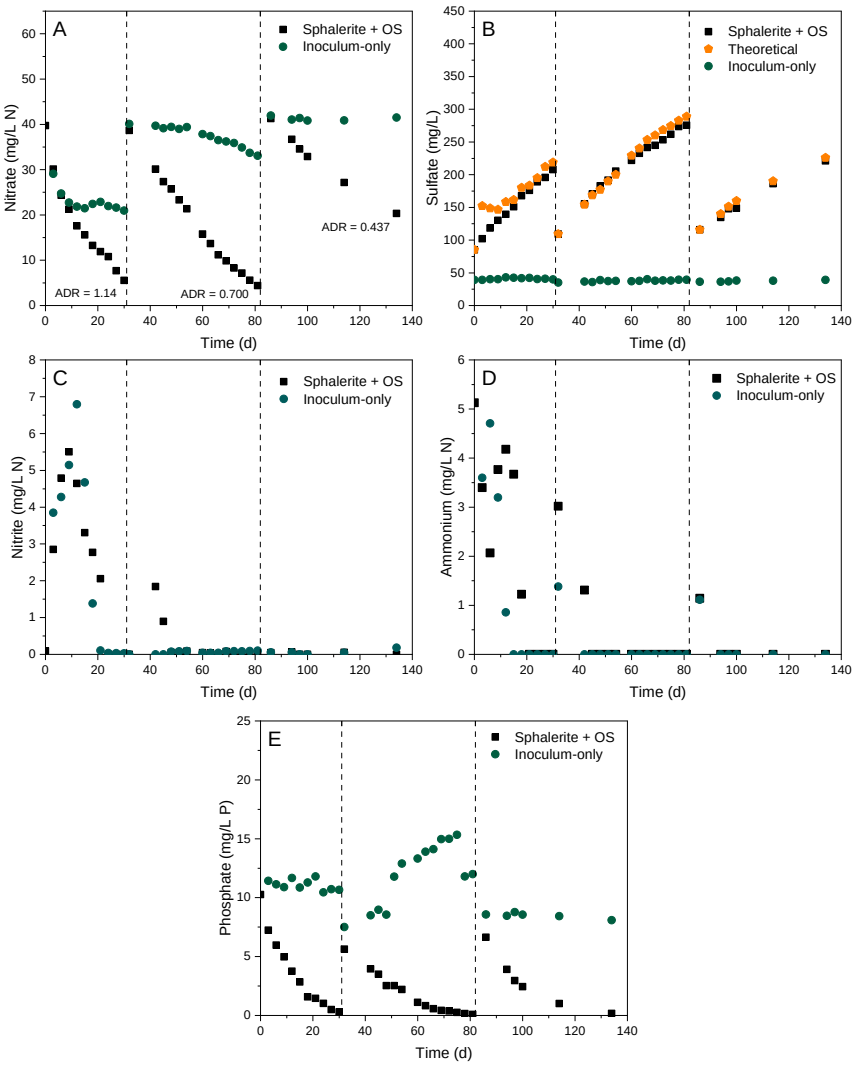
A
Sphalerite + OS
Inoculum-only
Nitrate (mg/L N)
ADR = 1.14
ADR = 0.700
ADR = 0.437
Time (d)
B
Sphalerite + OS
Theoretical
Inoculum-only
Sulfate (mg/L)
Time (d)
C
Sphalerite + OS
Inoculum-only
Nitrite (mg/L N)
Time (d)
D
Sphalerite + OS
Inoculum-only
Ammonium (mg/L N)
Time (d)
E
Sphalerite + OS
Inoculum-only
Phosphate (mg/L P)
Time (d)

662

663 Fig. 4

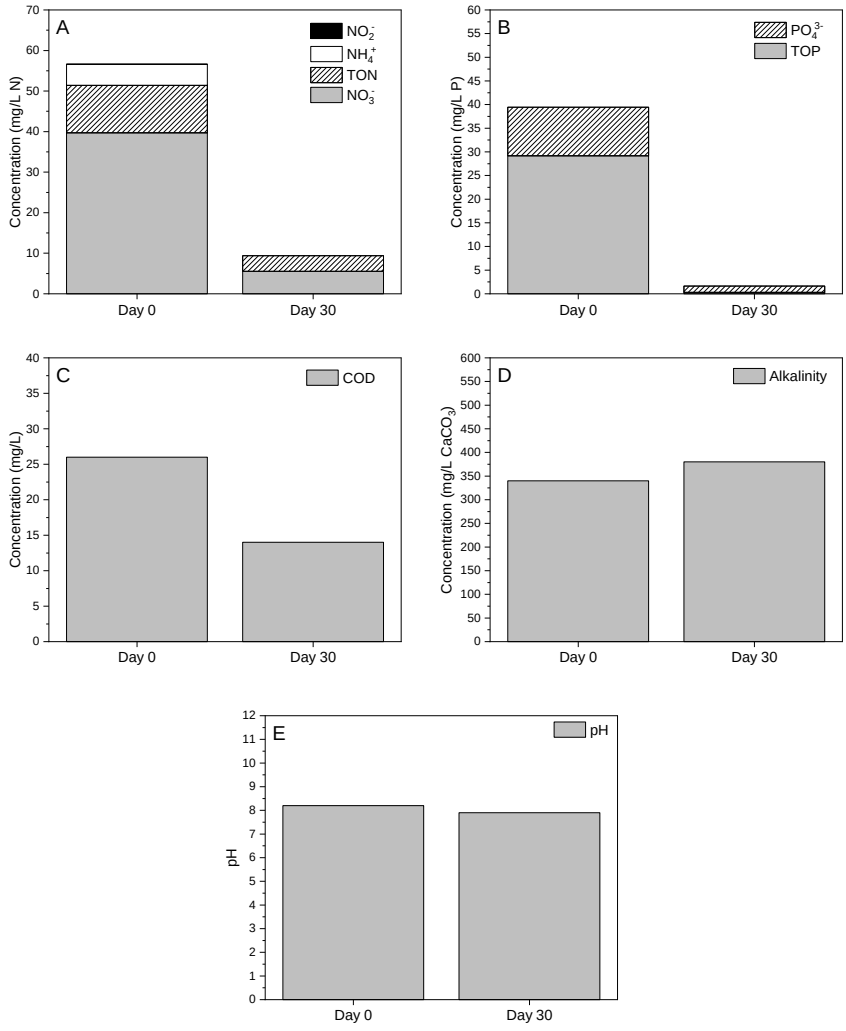

664
665

Fig. 5

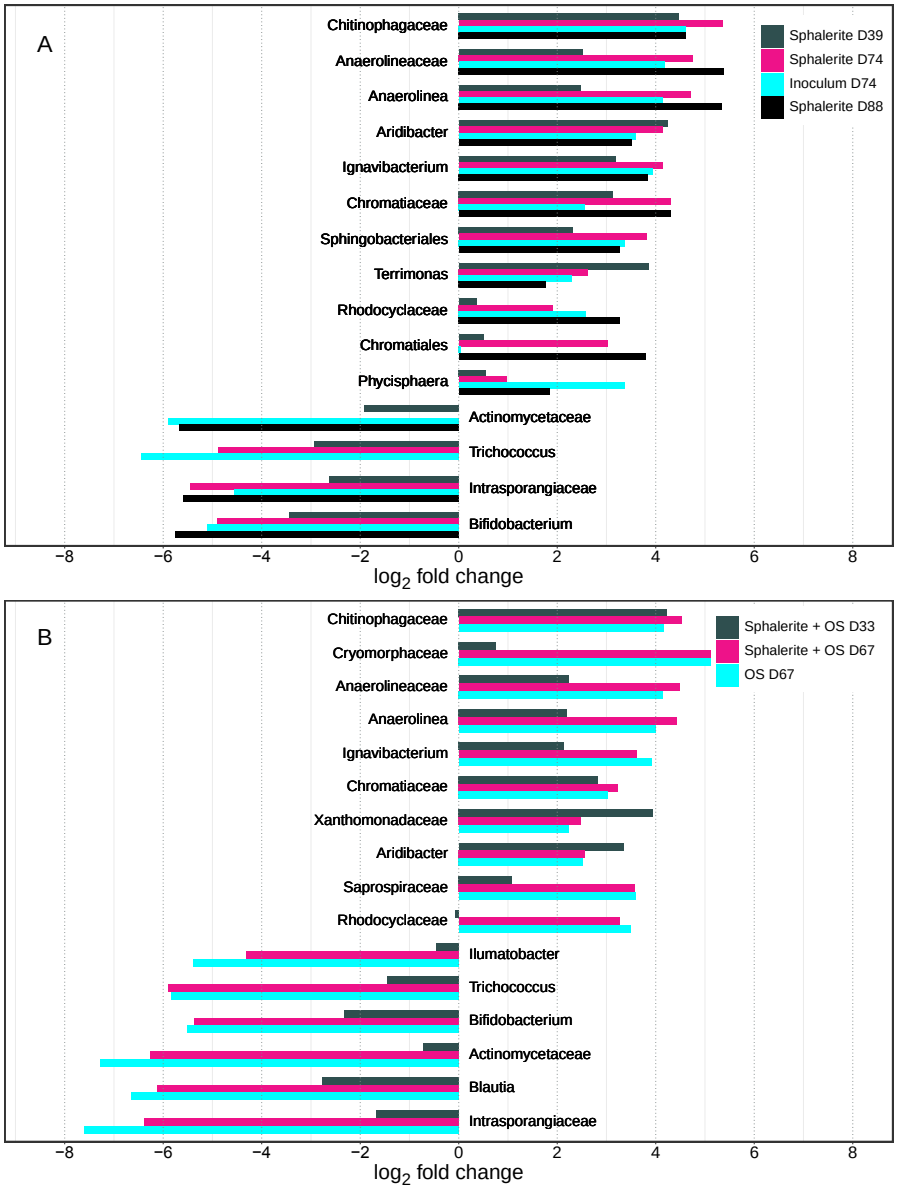
A
Chitinophagaceae
Anaerolineaceae
Anaerolinea
Aridibacter
Ignavibacterium
Chromatiaceae
Sphingobacteriales
Terrimonas
Rhodocyclaceae
Chromatiales
Phycisphaera
Actinomycetaceae
Trichococcus
Intrasporangiaceae
Bifidobacterium
Sphalerite D39
Sphalerite D74
Inoculum D74
Sphalerite D88
−8 −6 −4 −2 0 2 4 6 8
log2 fold change
B
Chitinophagaceae
Cryomorphaceae
Anaerolineaceae
Anaerolinea
Ignavibacterium
Chromatiaceae
Xanthomonadaceae
Aridibacter
Saprospiraceae
Rhodocyclaceae
Ilumatobacter
Trichococcus
Bifidobacterium
Actinomycetaceae
Blautia
Intrasporangiaceae
Sphalerite + OS D33
Sphalerite + OS D67
OS D67
−8 −6 −4 −2 0 2 4 6 8
log2 fold change

Fig. 6

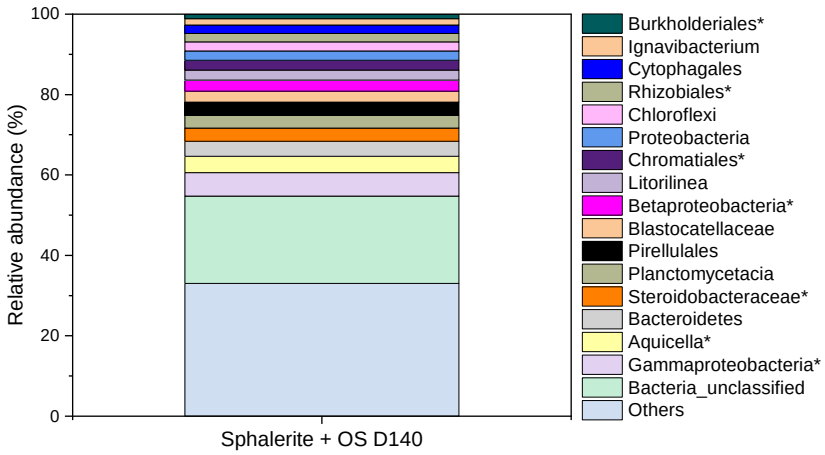
Relative abundance (%)
100
80
60
40
20
0
Sphalerite + OS D140
Burkholderiales*
Ignavibacterium
Cytophagales
Rhizobiales*
Chloroflexi
Proteobacteria
Chromatiales*
Litorilinea
Betaproteobacteria*
Blastocatellaceae
Pirellulales
Planctomycetacia
Steroidobacteraceae*
Bacteroidetes
Aquicella*
Gammaproteobacteria*
Bacteria_unclassified
Others

Table 1 Batch denitrification study details. Note: S^0 = Elemental Sulfur; OS = Oyster shells; UN = Uninoculated.

	Phase 1	Phase 2	Phase 3
Description:	Sphalerite-based autotrophic denitrification of groundwater	Effect of combined sphalerite & oyster shells on nutrient removal from groundwater	Effect of sphalerite & oyster shell dose on nutrient removal from domestic wastewater
Liquid volume (mL)	100	100	900
Duration (d)	88	67	140
Experimental Reactors	Sphalerite (12 g)	Sphalerite + OS (12 g; 4 g) OS (4 g)	Sphalerite + OS (Cycle 1: 164 g; 41 g) (Cycles 2 & 3: 258 g; 47 g)
Control Reactor(s)	Inoculum-only S^0 + OS (12 g + 4 g) Sphalerite UN (12 g)	Inoculum-only OS UN (4 g)	Inoculum-only
Sample collection for microbial community analysis	Days 0, 39, 74, 88	Days 0, 33, 67	Day 140

711 **Table 2** Relative abundance of notable bacteria identified in Phase 1 and 2. UD = undetected.
712

Phase 1	*Chromatiaceae*	*Chromatiales*	*Thiobacillus*	*Candidatus Kueneia*	*Candidatus Brocadiaceae*	*Ignavibacterium*
Sphalerite D39	0.32%	0.044%	0.24%	UD	UD	1.6%
Sphalerite D74	0.71%	0.25%	0.19%	UD	UD	3.2%
Inoculum D74	0.21%	0.032%	0.003%	0.057%	UD	2.8%
Sphalerite D88	0.71%	0.43%	0.43%	0.054%	UD	2.6%
Phase 2	*Chromatiaceae*	*Chromatiales*	*Thiobacillus*	*Candidatus Kueneia*	*Candidatus Brocadiaceae*	*Ignavibacterium*
Sphalerite + OS D33	0.26%	0.055%	0.083%	UD	UD	0.80%
Sphalerite + OS D67	0.34%	0.036%	0.009%	0.35%	0.94%	2.2%
OS D67	0.25%	0.080%	0.007%	1.0%	0.14%	2.7%

713

Declaration of interests

☒The authors declare that they have no known competing financial interests or personal relationships that could have appeared to influence the work reported in this paper.

☐The authors declare the following financial interests/personal relationships which may be considered as potential competing interests:

CRediT author statement

Erica A. Dasi: Conceptualization, Methodology, Investigation, Formal analysis, Writing - original draft, Writing - review & editing, Funding acquisition.

Jeffrey A. Cunningham: Conceptualization, Writing - review & editing, Funding acquisition.

Emmanuel Talla: Conceptualization, Methodology, Formal Analysis, Writing - original draft, Writing - review & editing, Supervision, Project administration, Funding acquisition.

Sarina J. Ergas: Conceptualization, Methodology, Writing - original draft, Writing - review & editing, Supervision, Project administration, Funding acquisition.

Click here to access/download
Electronic Annex
Appendix_Supplementary materials Revised 022023.docx